Article

Cell Chemical Biology

LRP-1 links post-translational modifications to efficient presentation of celiac disease-specific T cell antigens

Graphical abstract

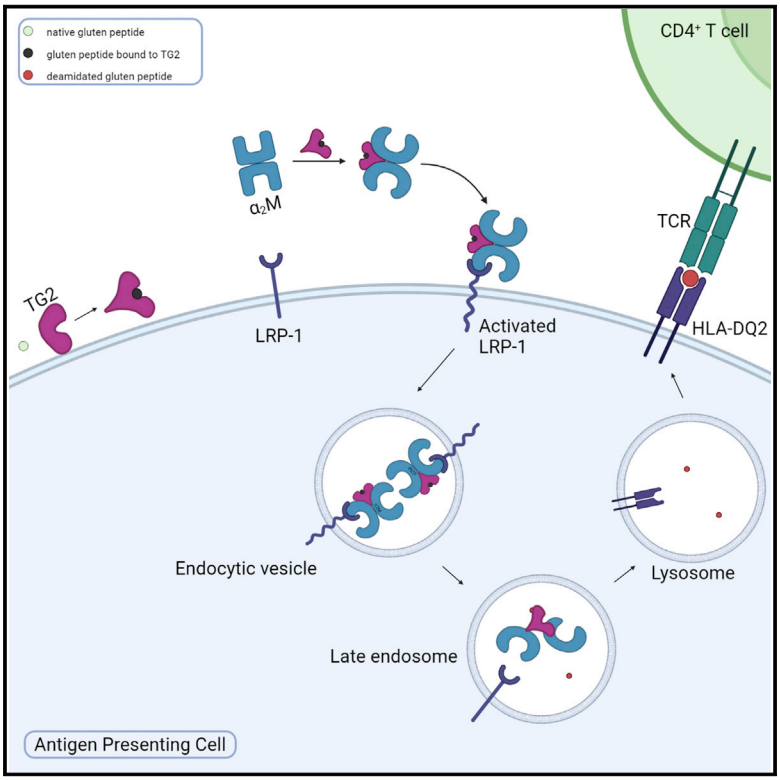

Highlights

- Endocytosis of gluten antigens depends on transglutaminase-2 and α_2-macroglobulin
- LRP-1 mediates uptake, causing lysosomal concentration of deamidated gluten peptides
- Peptidomimetic active TG2 probes allow tracking of TG2 through the endolysosome
- Antigens taken up through this pathway are presented on MHC-II in a DQ2 restricted way

Authors

Elise Loppinet, Harrison A. Besser, Agnele Sylvia Sewa, Fu-Chen Yang, Bana Jabri, Chaitan Khosla

Correspondence

khosla@stanford.edu

In brief

Loppinet et al. demonstrate that gluten peptides bound to TG2 undergo LRP-1-mediated endocytosis in the presence of α_2-macroglobulin. Deamidated gluten peptides are then concentrated in the endolysosomal system and efficiently displayed on MHC-II in HLA-DQ2-expressing cells. This invokes a pathogenic role for macrophages and dendritic cells in celiac disease.

Loppinet et al., 2023, Cell Chemical Biology *30*, 55–68
January 19, 2023
https://doi.org/10.1016/j.chembiol.2022.12.002

CellPress

Cell Chemical Biology

CellPress

Article

LRP-1 links post-translational modifications to efficient presentation of celiac disease-specific T cell antigens

Elise Loppinet,[1] Harrison A. Besser,[2,3] Agnele Sylvia Sewa,[4] Fu-Chen Yang,[2] Bana Jabri,[5] and Chaitan Khosla[1,2,6,7,*]
[1]Department of Chemical Engineering, Stanford University, Stanford, CA 94305, USA
[2]Department of Chemistry, Stanford University, Stanford, CA 94305, USA
[3]Stanford Medical Scientist Training Program, Stanford University School of Medicine, Stanford, CA 94305, USA
[4]Department of Biochemistry, Stanford University School of Medicine, Stanford, CA 94305, USA
[5]Department of Medicine, University of Chicago, Chicago, IL 60637, USA
[6]Sarafan ChEM-H, Stanford University, Stanford, CA 94305, USA
[7]Lead contact
*Correspondence: khosla@stanford.edu
https://doi.org/10.1016/j.chembiol.2022.12.002

SUMMARY

Celiac disease (CeD) is an autoimmune disorder in which gluten-derived antigens trigger inflammation. Antigenic peptides must undergo site-specific deamidation to be presentable to CD4$^+$ T cells in an HLA-DQ2 or -DQ8 restricted manner. While the biochemical basis for this post-translational modification is understood, its localization in the patient's intestine remains unknown. Here, we describe a mechanism by which gluten peptides undergo deamidation and concentration in the lysosomes of antigen-presenting cells, explaining how the concentration of gluten peptides necessary to elicit an inflammatory response in CeD patients is achieved. A ternary complex forms between a gluten peptide, transglutaminase-2 (TG2), and ubiquitous plasma protein α_2-macroglobulin, and is endocytosed by LRP-1. The covalent TG2-peptide adduct undergoes endolysosomal decoupling, yielding the expected deamidated epitope. Our findings invoke a pathogenic role for dendritic cells and/or macrophages in CeD and implicate TG2 in the lysosomal clearance of unwanted self and foreign extracellular proteins.

INTRODUCTION

Celiac disease (CeD) is an autoimmune disease that affects approximately 1% of the population in most parts of the world.[1] Ingestion of gluten proteins from wheat, barley, or rye by a CeD patient induces widespread inflammation, including T cell inflammation in the small intestinal mucosa, leading to villous atrophy and symptoms ranging from abdominal pain and bloating to chronic fatigue, anemia, and osteopenia.[2] In contrast to most other autoimmune diseases, the primary environmental and genetic factors causing CeD, dietary gluten and HLA-DQ2 or -DQ8, respectively, have been identified and their pathologically relevant interactions have been characterized in considerable depth.[3] However, other than strict, lifelong gluten exclusion, there is currently no approved therapy for CeD.[4]

An extensive body of evidence has established that sequence-selective deamidation of gluten peptides by transglutaminase-2 (TG2; Figures 1A and 1B) is necessary for their high-affinity recognition by disease-associated HLA-DQ2 or -DQ8 and subsequent presentation to CD4$^+$ T cells.[7] TG2 is a ubiquitous enzyme found in intracellular as well as extracellular compartments of the mammalian intestine; its activity is upregulated in response to dietary gluten in a transgenic mouse model of CeD.[8] Together, these observations provide a compelling molecular rationale for the onset of gluten-dependent inflammation in CeD. For example, a 33-residue peptide, LQLQPFPQP**Q**LPYPQP**Q**LPYPQP**Q**LPYPQ PQPF, generated via chymotrypsin-catalyzed proteolysis of dietary gluten in the upper intestinal lumen, undergoes TG2-promoted deamidation at the boldfaced residues to reveal multiple copies of DQ2-restricted T cell epitopes.[9,10] Upon surface presentation by DQ2-expressing antigen-presenting cells (APCs), the deamidated peptide potently activates disease-specific T-helper cells.[11]

However, a fundamental remaining mystery in our knowledge of CeD pathogenesis concerns how the threshold for induction of pathogenic CD4$^+$ T cell responses is reached. The need for such a threshold is supported by the presence of an HLA-gene dosage effect for CeD susceptibility,[12] the observation that HLA-DQ2, which has the potential to bind a higher number of gluten peptides than HLA-DQ8, is the strongest disease determinant,[13] and the requirement of deamidation for tissue destruction.[8] Simple diffusion-driven encounters between extracellular gluten peptides and MHC proteins expressed by APCs, while theoretically possible, are unlikely to result in sufficient numbers of MHC-deamidated gluten peptide complexes to induce pathology for two reasons. First, gluten peptide concentration in the sub-epithelial environment of the small intestine is expected

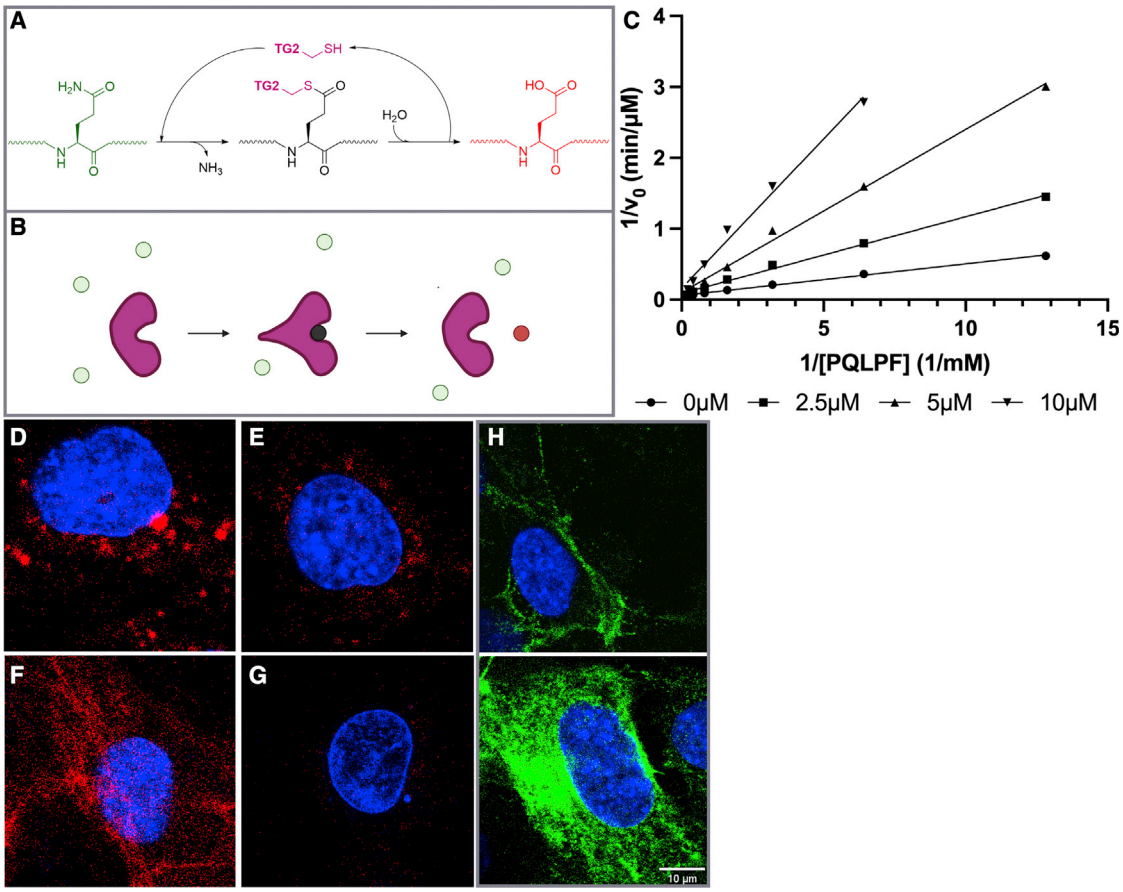

Figure 1. Relevant properties of transglutaminase-2

(A) Transglutaminase-2 (TG2)-catalyzed conversion of a gluten peptide (green) into a high-affinity deamidated analog (red) via a transient covalently bound thioester species (black).

(B) Cartoon representation of the transformation shown in (A). The covalent acyl-enzyme intermediate is anticipated to undergo a transient conformational change.[5]

(C) Kinetic analysis of TG2 inhibition by HB225. Both substrate (PQLPF) and inhibitor concentrations were varied. Measurements were done in triplicate (n = 3).

(D–G) Probing mouse embryonic fibroblasts (MEFs) with HB230 and related probes of TG2 activity. (D) Treatment of wild-type MEFs with 1 μM HB230 in the presence of 10 μM thioredoxin (TRX)—needed to activate latent extracellular TG2 in this cell line[6]—leads to a punctate staining pattern that is markedly diminished in TG2 knockout MEFs (E). (F) The staining pattern of HB230 is distinct from that observed with 100 μM 5BP, which elicits a fibrous incorporation pattern that highlights fibronectin strands in the extracellular matrix.[6] (G) HB230 labeling of MEFs is fully inhibited by co-treatment with 10μM CK805, a reference TG2 inhibitor.

(H) Staining using an anti-TG2 antibody uncovers localization of the protein in live (top) and fixed/permeabilized cells (bottom). TG2 is abundant on the cell surface as well as intracellular compartments. For a wide view, see Figure S1. In all panels, blue staining is DAPI and green is TG2 protein. Red staining is 5BP in (F) and HB230 in all other panels.

to be significantly lower than the K_M values of TG2 (10–100 μM) even for the most favored substrates. This would be especially so after relatively minor but nonetheless inflammatory dietary lapses by CeD patients, which deliver 0.1–1 g gluten (~1 μM of the aforementioned 33-residue peptide) into the duodenal lumen; from there a further concentration drop presumably results across the epithelium due to the barrier-like properties of tight junction proteins. Second, because class II MHCs are typically loaded with peptide ligands in the late endosome or lysosome,[14] a mechanism must exist to enrich deamidated gluten antigens in this compartment of APCs.

Several subsets of APCs have been observed in the mucosa of CeD patients, including $CD123^+$ and $CD11^+$ dendritic cells and $CD68^+$ macrophages.[15–18] However, their role in CeD pathogenesis remains unclear, because deamidated gluten peptides are not expected to accumulate in the lamina propria of the small intestine to be spontaneously engulfed via pinocytosis by these cells in pathologically meaningful quantities.[14] While it is possible that some antigen is sampled by dendritic cells at the epithelial surface or via M cell transport,[19] alternative mechanisms must also be considered for APCs to selectively endocytose the deamidated gluten peptides and concentrate them in lysosomes for efficient MHC-II presentation. Here we describe a mechanism for gluten presentation that relies on high-affinity protein-protein interactions while simultaneously enabling lysosomal enrichment of deamidated gluten antigens.

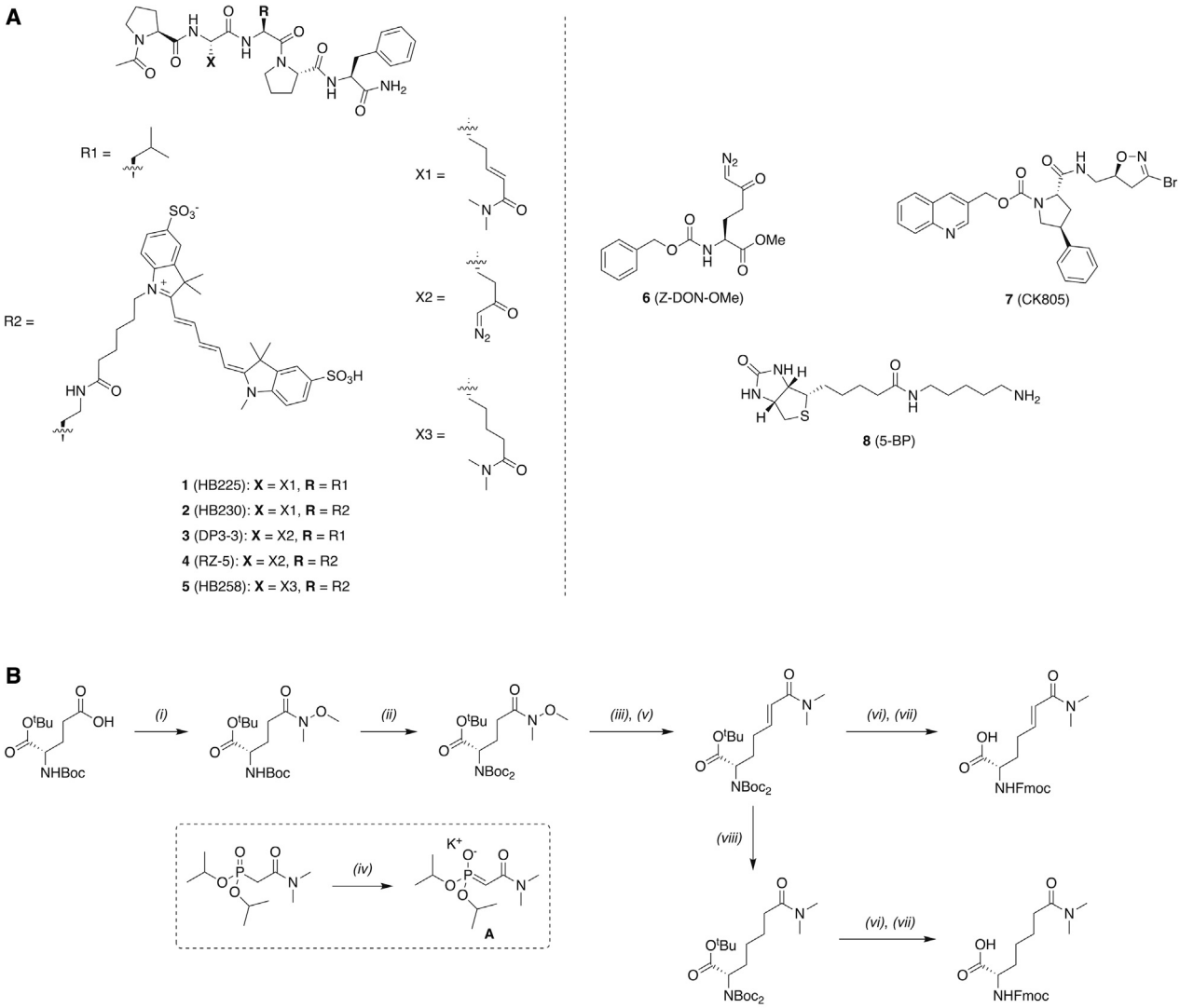

(i) HNMeOMe·HCl, IBCF, NMM, DCM, 0°C→RT, 3 hrs (93%) *(ii)* Boc_2O, NEt_3, DMAP, DCM, reflux, 3 hrs (97%) *(iii)* DIBAL-H, THF, -78°C→RT, 1 hr *(iv)* KO^{t}Bu, THF, 30 mins, RT
(v) **A**, THF, RT, 1.5 hrs (78%, >40:1 *E:Z*, 2 steps) *(vi)* 1:1 TFA/DCM, RT, 4 hrs *(vii)* Fmoc-OSu, DIPEA, DCM, 30 mins (88%, 2 steps) *(viii)* $NaBH_4$, $CoCl_2{\cdot}6H_2O$, MeOH, 0°C→RT, 30 mins (96%)

IBCF: isobutyl chloroformate, NMM: N-methylmorpholine, DIBAL-H: diisobutylaluminum hydride, DMAP: 4-dimethylaminopyridine, Boc_2O: ditertbutyl dicarbonate, DCM: dichloromethane, THF: tetrahydrofuran

Scheme 1. Structures and syntheses of relevant small molecules
(A) Structures of key small molecules used in this study.
(B) Synthesis of HB230 and HB258.

RESULTS

Our quest to elucidate the mechanistic basis for gluten antigen delivery to HLA-DQ2 or -DQ8 was initiated by engineering a high-affinity probe to directly visualize the location of active TG2 in the small intestine. Prior work has shown that a vast majority of TG2 in the extracellular matrix of the small intestine is catalytically inactive and that inflammatory signals are required to induce enzyme activity.[6,20,21] We hypothesized that active TG2 in the CeD small intestine would be non-uniformly distributed and may thus highlight the precise location where MHC binds to deamidated gluten peptides. While small molecule probes of TG2 activity have previously been reported, none of them have the requisite selectivity to visualize the active enzyme *in situ* with high spatial resolution.[22] The most widely used example of a TG2 activity probe, 5-biotinamidopentylamine (5-BP), is a relatively weak nucleophilic substrate, which becomes attached to electrophilic Gln (Q) residues of matrix protein substrates such as fibronectin[23] when dosed at high concentrations (>100 μM in cell culture or >100 mg/kg intravenously in mice).[20,24] In all experiments involving the use of 5-BP to visualize TG2, it has been assumed that the enzyme co-localizes with its substrates, but this assumption has never been experimentally tested.

Design, synthesis, and biochemical analysis of HB230

HB225 (**1**, Scheme 1A) is a peptidomimetic small molecule modeled after the TG2 recognition site of its preferred substrate PQLPY, three copies of which are found in the 33-residue gluten

peptide cited above. Upon deamidation, each site exposes two overlapping $CD4^+$ T cell epitopes, P(F/Y)PQP**E**LPY and PQP**E**LPYPQ, known to be immunodominant in HLA-DQ2-expressing CeD patients. Three key features were central to the design of HB225. First, the reactive Gln residue of P**Q**LPY was replaced with an isosteric unnatural amino acid harboring an α,β-unsaturated dimethylamide "soft" electrophile, which was expected to result in irreversible covalent attachment of this small molecule inhibitor to the active site Cys residue (C277) of TG2 via a Michael addition. (This unnatural amino acid will hereafter be referred to as HWE in recognition of the Horner-Wadsworth-Emmons reaction that was central to its gram-scale synthesis.) Second, the terminal Tyr (Y) residue was replaced with proteinogenic Phe (F) for synthetic convenience, as the phenolic substituent of Tyr was also not predicted to be relevant to TG2 or HLA-DQ2[5,10] recognition based on co-crystal structures of both proteins solved previously in our laboratory. And finally, the N- and C-termini of HB225 harbored acetyl and amide protecting groups, respectively, to mimic the context of a longer peptide while also mitigating amino- and carboxy-peptidase catalyzed destruction of the probe in the proteolytically harsh gastrointestinal lumen.

Synthesis of HB225 is outlined in Scheme 1B and described in the STAR Methods section. Steady-state kinetic analysis (Figure 1C) revealed that HB225 inactivated human TG2 with high specificity (k_i = 0.04 min^{-1}, K_i = 1.3 μM), comparable to the most potent irreversible inhibitor reported to date, DP3-3 (**2**; Scheme 1A), which harbors a 6-diazo-5-oxo-norleucine (DON) warhead in place of a reactive Gln.[5] Encouraged by this finding, we went on to design and synthesize our target fluorescent probe, HB230 (**3**, Scheme 1A), in which a second unnatural amino acid residue, diaminobutyrate (DAB), was installed in place of Leu (L) in HB225. This residue was also predicted to not be recognized by TG2. Attachment of a Sulfo-Cy5 fluorophore via NHS-ester linkage to the DAB residue yielded the desired probe. As anticipated, HB230 had comparable potency to HB225 (IC_{50} = 4.9 versus 5.1 μM, respectively, under equivalent assay conditions, Figure S1A). We also synthesized a small quantity of RZ-5 (**4**; Scheme 1A), an analog of HB230 harboring the DON residue in place of HWE. RZ-5 was comparably potent to HB230 but was not subjected to extensive biological evaluation due to its lack of synthetic scalability and lability under simulated acidic conditions of the stomach.

HB230 reveals a novel pattern of active TG2 localization

Incubation of mouse embryonic fibroblasts (MEFs) with HB230 for 3 h led to labeling of these cells in a manner that was not observed with control MEFs derived from TG2-knockout mice (Figures 1D–1G). Similar results were also obtained when treating with RZ-5 (Figure S1B). Notably, both probes revealed a hitherto unprecedented labeling pattern that was markedly different from equivalent experiments in which 5-BP was used to visualize TG2 activity (Figure 1F); whereas the latter samples showed the label bound to extracellular matrix proteins (e.g., fibronectin) in a predictably fibrous pattern, the former samples showed predominantly punctate, intracellular labeling that was primarily located near the nucleus. Labeling was strongly dependent in all cases upon addition of recombinant human thioredoxin (TRX) to the culture medium for the duration of the HB230 treatment[6]; TRX activates extracellular TG2 via reduction of a disulfide bond between C370 and C371 that allosterically maintains the enzyme in an inactive state. TG2 is ubiquitously expressed and found in both intracellular and extracellular spaces (Figure 1H). While it is not clear what the distribution is between membrane bound and diffusible free TG2 in the extracellular environment, there appears to be sufficient TG2 near the membrane (Figure 1H, top) to generate the activity observed in Figures 1D and 1F. As expected, addition of the TG2-selective inhibitor CK805[25] led to a sharp reduction in fluorescent labeling of HB230 (Figure 1G). Together, these preliminary results suggested that, whereas activated TG2 predominantly recognized and modified protein substrates localized to the extracellular matrix of cells, the active enzyme itself was efficiently internalized via an endocytic process. Our data were uncannily reminiscent of reports from Pastan and coworkers over 4 decades ago, who concluded that TG2 activity is essential in receptor-mediated endocytosis of certain physiologically important proteins such as α_2-macroglobulin (α_2M), insulin, and epidermal growth factor.[26,27] To our knowledge however, those authors' remarkable observations have not been subsequently followed up in detail.

HB230 induces α_2-macroglobulin-dependent endocytosis of catalytically active TG2

The ~800 kDa homotetrameric pan-protease inhibitor, α_2-macroglobulin (α_2M), is present at high concentrations in human plasma (1–5 mg/mL) and presumably also in the extracellular environments of most cells.[28] Rather than directly inhibiting enzyme activity, α_2M acts by collapsing around its target proteases through a large-scale conformational change, in turn becoming recognizable by low-density lipoprotein receptor-related protein 1 (LRP-1) and undergoing canonical receptor-mediated endocytosis,[29] eventually leading to endolysosomal protease destruction and receptor recycling. Because serum-containing culture media invariably contains a low and variable amount of α_2M, we systematically investigated the effect of α_2M supplementation on HB230-mediated endocytosis of TG2. Normal rat kidney (NRK) cells were used in these and several subsequent experiments, because earlier work by Pastan and coworkers[26,27] had predominantly relied on the use of this non-cancerous cell line. As seen in Figure 2A, NRK cells showed robust uptake of 1 μM exogenous HB230 in 90 min. Uptake was independent of exogenous TRX addition, suggesting the existence of a relatively high innate extracellular TG2 activity level in cultures of this cell line. Puncta of two distinct sizes were observed. Supplementation of NRK cell cultures with α_2M led to a strong dose-dependent increase in uptake of HB230 up to ~100 μg/mL, indicative of a saturable mechanism. (Note that the physiological concentration of α_2M in human plasma typically exceeds 1 mg/mL.[30]) The addition of α_2M predominantly appeared to affect the size and number of the larger puncta, which are indicative of receptor-mediated endocytosis uptake.

To obtain definitive evidence for co-endocytosis of HB230 and α_2M, a fluorescent batch of α_2M was prepared as described in the STAR Methods section. Using this probe, a strong overlap was observed between the fluorescent signals of HB230 (red) and α_2M (green) in the larger, but not smaller, puncta (Figure 2B). Pearson's co-localization coefficient was calculated to quantify

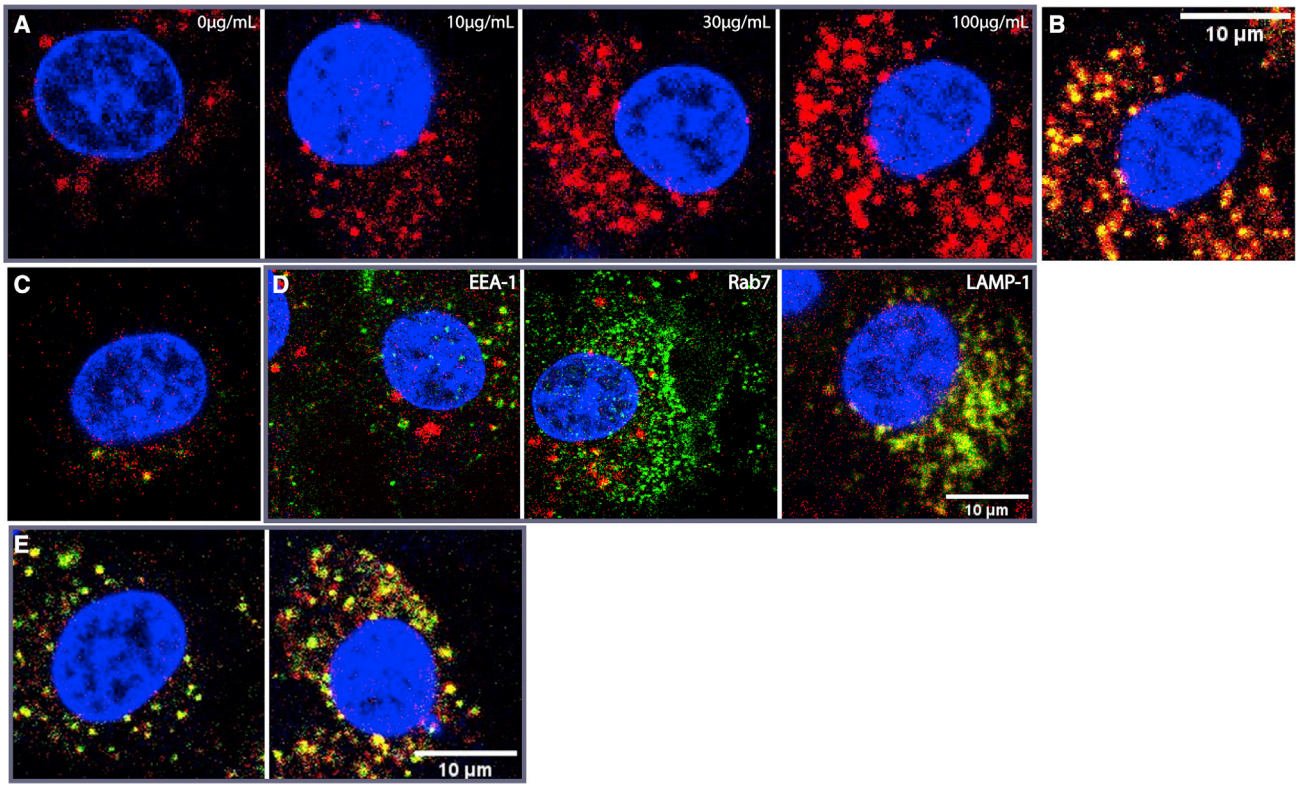

Figure 2. Characterization of HB230 and α_2M containing large puncta

(A) Dose-response of HB230 puncta to exogenous α_2M in cultures of NRK cells. In all panels, HB230 is present at a concentration of 1 μM. Uptake of TG2-bound HB230 increased with increasing doses of α_2M. When fluorescent α_2M is used, the overlap between HB230 (red) and α_2M (green) is strong (B).

(C) HB258 (1 μM) is internalized significantly less than HB230 even at saturating α_2M and the overlap between HB258 and the fluorescent α_2M is minimal.

(D) A labeled antibody (green) against the early endosome marker EEA-1 (left) shows non-overlapping localization in NRK cells relative to the compartment represented by large red puncta containing the HB230/TG2/α2M complex. Rab7 (middle, green) also does not colocalize strongly with HB230. In contrast, RFP-tagged LAMP-1 (lysosomal marker, green) strongly co-localizes with the same large red puncta (right).

(E) To assess the effect of lysosomal protease inhibition on probe clearance, HB230 (red) and labeled α_2M (green) were added to cultured NRK cells in the absence (left) or presence (right) of a cathepsin B inhibitor. After 90 min, the culture medium was replaced, and cells were incubated for an additional 30 min before visualizing via confocal microscopy. Inhibition of cathepsin B leads to an increase in the HB230/α_2M ratio, implying rapid proteolytic degradation of the peptidic TG2 inhibitor in the lysosome. For wide views of all panels in this figure, see Figure S2. In all panels, blue staining is DAPI and red staining is HB230. Green staining is as indicated in (D) and α_2M in (B) and (E).

the overlap between the red and green channels and was found to be PCC = 0.79 indicating a strong correlation.

To verify that HB230 internalization was dependent on TG2 activity, HB258 (**5**; Scheme 1A) was designed and synthesized as a control probe. This dihydro-analog is otherwise identical to HB230 but lacks its electrophilic warhead and is therefore unable to irreversibly bond to the active site C277 residue of TG2. The synthesis and biochemical characterization of HB258 are detailed in Figure 1B and the supplemental information. As seen in Figure 2C, HB258 does not undergo significant uptake by NRK cells even at high concentrations of both the probe and α_2M in the culture medium. Notably, this fluorescent probe only appears as small intracellular puncta; the larger puncta formed by HB230 are absent.

Characterizing the large puncta harboring co-localized TG2 and α_2M

To establish the identity of the large intracellular puncta harboring both α_2M and TG2 bound to HB230 (Figure 2A), NRK cells were transfected with a gene encoding lysosomal-associated membrane protein (LAMP-1) tagged to RFP. Wild-type and transfected cells were co-incubated with α_2M and HB230 for 90 min prior to fixation. To further characterize the large puncta containing both α_2M and TG2, fixed NRK cells were stained with an antibody against early endosome antigen-1 (EEA-1) and Rab7, a late endosomal marker. As observed in Figure 2D, EEA-1 and HB230 appear in distinct sub-cellular compartments for the most part (PCC = 0.01), implying that vesicles derived from internalization of the HB230/TG2/α_2M complex did not fuse with early endosomes. Similarly, Rab7 (Figure 2D, middle) also did not colocalize strongly with HB230 in the late endosomes (PCC = 0.03). In contrast, HB230 strongly co-localized with RFP-tagged LAMP-1 in the large puncta (Figure 2D, right, PCC = 0.426), implying that internalized vesicles harboring the ternary complex comprised of HB230, TG2 and α2M were efficiently escorted to the lysosome. Antigen processing prior to cell surface presentation occurs in different compartments, from early endosomes to lysosomes depending on the antigen and the cell

type, and antigens containing vesicles are not necessarily fused with endosomes.[31] Additionally, NRK cells are not professional APCs, and as a result may not have mature MHC-II presentation systems. Thus, it is likely that in these cells the substrate bound TG2 and α_2M complex is shuttled directly to lysosomal compartments without prior interaction with early or late endosomes.

Further evidence that the HB230/TG2/α_2M ternary complex is trafficked to the lysosome was derived by treating NRK cells with a cell-permeable cathepsin B inhibitor or vehicle along with HB230 and labeled α_2M (Figure 2E). Inhibition of this major lysosomal protease results in a prolonged lifespan of HB230 in this sub-cellular compartment, implying that the stable adduct formed between TG2 and this peptidic inhibitor is susceptible to proteolytic clearance from the lysosome.

Recognition of TG2 by α_2M

TG2 activity is regulated by multiple allosteric mechanisms.[32,33] Most notably, while binding of multiple Ca^{2+} ions is required for transamidation or deamidation activity,[34,35] enzymatic activity is fully inhibited by either guanine nucleotide binding or the reversible formation of an allosteric C370-C371 disulfide bond.[36] Independently, X-ray crystallographic analysis has identified at least two markedly distinct conformational states of the 78 kDa protein – a "closed" GTP-bound form and an "open" state revealed through inactivation of the enzyme with DP3-3.[5] Whereas the latter state allowed direct visualization of the C370-C371 disulfide bond, this bond was reduced in the GTP-bound state. A parsimonious model for TG2 catalysis assumes that the active enzyme is in the open state or a closely related conformation, although limitations of this model have been noted.[37]

To identify the conformational requirements for high-affinity recognition of TG2 by α_2M, fluorescently labeled α_2M was added to NRK cell cultures in the presence of a representative set of (unlabeled) TG2 inhibitors whose biochemical mechanisms have been previously analyzed in our laboratory.[5] As shown in Figure 3A, in the absence of any exogenous TG2 probe, labeled α_2M was only internalized as small puncta, analogous to those observed with HB258 (Figure 2B). In contrast, both HB225, and Z-DON-OMe (**6**, a commercially available weaker analog of DP3-3; Scheme 1A) promoted dose-dependent formation of larger α_2M-labeled puncta. As expected, a higher concentration of Z-DON-OMe was required to elicit this behavior (Figure 3B versus Figure 3C), consistent with its lower inhibitory potency against TG2. Together, these observations suggested that TG2 recognition by α_2M requires active site occupancy. Two additional small molecule probes were evaluated. First, CK805 (**7**, Scheme 1A) is a non-peptidic irreversible inhibitor of TG2.[25] Notwithstanding its ability to covalently bind to the active site C277 residue of the enzyme, it does not induce a crystallizable open conformation (unpublished results). Addition of CK805 to NRK cell cultures in conjunction with fluorescent α_2M did not stimulate fluorophore internalization (Figure 3D). Second, cystamine is a small molecule oxidant that inactivates TG2 by promoting C370-C371 disulfide bond formation even in the absence of active site occupancy[36]; it too was unable to promote rapid internalization of fluorescent α_2M by itself (Figure 3E). Together, our data suggest that α_2M-promoted endocytosis requires active site occupancy by a substrate or inhibitor that can stabilize the structurally characterized open conformer of TG2.

Direct biochemical evidence for ligand-dependent recognition of TG2 by α_2M was obtained using purified recombinant human TG2 expressed in *E. coli* and α_2M expressed recombinantly in mammalian cells, as detailed in the STAR Methods section. In the presence of α_2M, a decrease was measured in the k_{cat} of TG2 for Ac-PQLPF-NH_2 (the substrate analog of HB225; 35 ± 1 min^{-1} versus 29 ± 1 min^{-1}) but not CBz-QG (a commonly used albeit lower-affinity reference substrate; 21 ± 2 min^{-1} versus 21 ± 1 min^{-1}), consistent with a non-competitive inhibition mechanism of TG2 by α_2M (Figure S4A). Whereas TG2-mediated activation of α_2M does not require concomitant enzyme inhibition, its observation is indicative of physical interaction between the two proteins. Inhibition was abolished when truncated but catalytically active TG2 derivatives lacking the C-terminal β-barrel domain were assayed (Figure S4B). Specifically, the k_{cat} values of a derivative lacking the C-terminal β-barrel domain[38] were 9 ± 1 min^{-1} and 8 ± 1 min^{-1} in the absence or presence, respectively, of α_2M. Similarly, the k_{cat} values of a derivative harboring the N-terminal and catalytic domains but lacking both β-barrel domains[38] were 7 ± 0.2 min^{-1} and 7 ± 0.3 min^{-1} in the absence or presence, respectively, of α_2M (Figure S4C). Together, these findings support a mechanistic model in which α_2M interacts directly with the C-terminal β-barrel domain of TG2 but only in the presence of a high-affinity substrate.

Endocytosis of antigenic gluten peptides via ternary complex formation

Thus far, endocytosis of the TG2-α_2M complex has exclusively been visualized using peptidic probes that irreversibly label the active site of TG2. However, in the context of CeD, gluten peptides undergo transient attachment to C277 via a thioester linkage that is subsequently hydrolyzed (Figure 1B). To investigate whether this transient enzyme-substrate complex can be recognized by α_2M under physiologically relevant conditions, NRK cells were co-incubated with fluorescent α_2M and the aforementioned 33-residue gluten peptide (33mer) tagged with a Cy5 fluorophore. The native 33mer was taken up in a dose-dependent manner (Figures 3F and 3J), whereas internalization of its deamidated counterpart was substantially less efficient (Figure 3G), underscoring the importance of forming the thioester bond between TG2 and its substrate in this process. Increasing the concentration of fluorescently labeled α_2M led to a corresponding increase in endocytosis of the 33mer peptide. An entirely analogous pattern of co-localized endocytosis was observed between these two fluorescent probes (Figure 3I) as between α_2M and HB230. Notably, while both probes underwent independent uptake as small puncta, their co-localization was restricted to the large puncta. Even more remarkably, the dose-dependent effect of the 33mer saturates at low micromolar concentrations, considerably below the K_M of TG2 for this peptide.[9]

Fibronectin is generally considered as a prototypical extracellular substrate of TG2.[39,40] We therefore sought to establish whether a ternary complex between fibronectin, TG2 and α_2M could also be internalized analogously to the 33mer gluten peptide. As seen in Figure 3H, endocytosis of extracellular

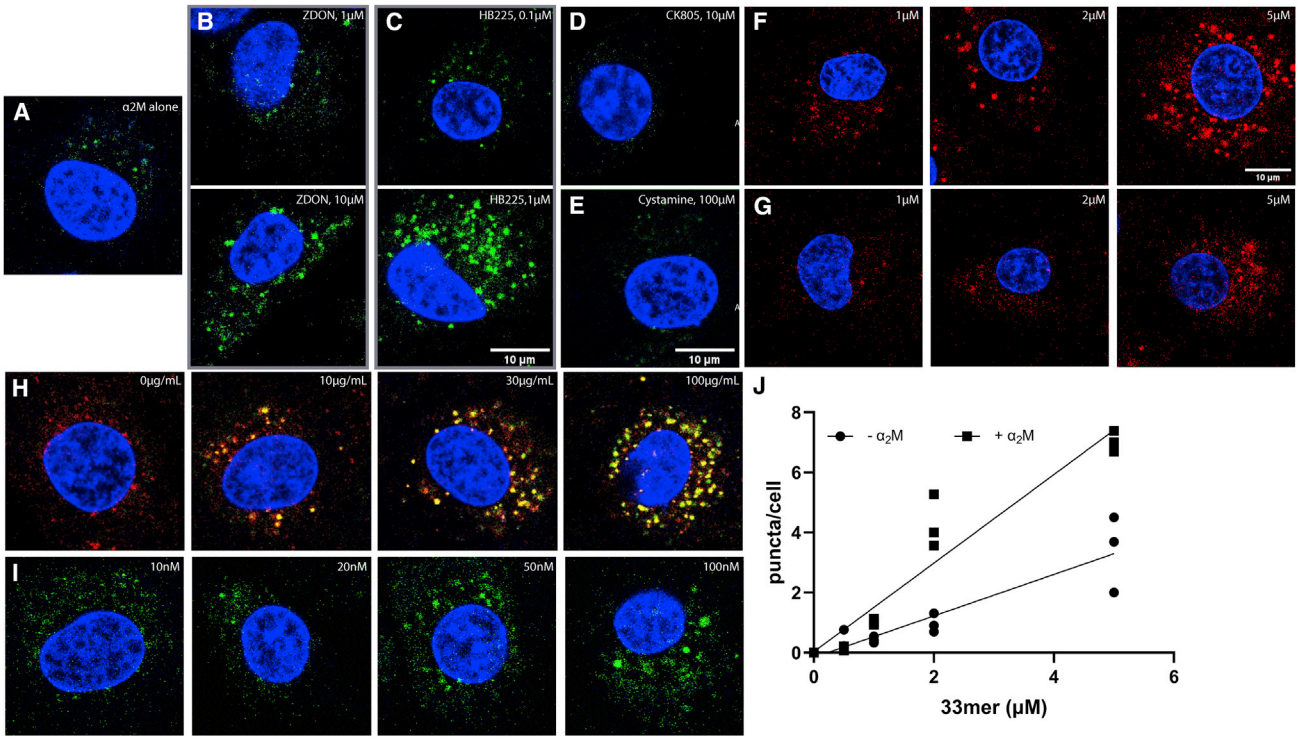

Figure 3. Dependence of α_2M endocytosis on the mechanism of TG2 inhibition

(A) Fluorescent α_2M (green) undergoes limited endocytosis in the absence of any exogenous TG2 probe; labeled α_2M is predominantly internalized as small puncta comparable in size to the smaller puncta observed in Figure 2.

(B) Co-treatment with Z-DON-OMe shows a dose-dependent increase in the appearance of larger labeled puncta in the 1–10-μM concentration range of this TG2 inhibitor.

(C) HB225 has an analogous, more pronounced effect, albeit at lower concentrations of the probe. Two unrelated TG2 inhibitors, CK805 (D, 10 μM) and cystamine (E, 100 μM) do not yield the larger puncta at saturating concentrations, although small α_2M-labeled puncta are observed. In all samples, α_2M was added at 100 μg/mL concentrations.

(F and G) Co-incubation of 100 μg/mL α_2M causes increased uptake of a fluorescent analog of the native 33mer gluten-derived peptide (F) compared with its deamidated counterpart (G), which is not significantly internalized by NRK cells.

(H) Increasing the concentrations of exogenous a$_2$M in the presence of 1 μM 33mer increases uptake of both the 33mer (fluorescently labeled with Sulfo-Cy5) and α_2M. Under all conditions, co-localization of the two labeled probes appears to be restricted to the large puncta.

(I) Co-incubation of 100 μg/mL fluorescently labeled α_2M in the presence of increasing concentrations of exogenously added fibronectin results in a dose-dependence increase in the abundance of large but not small puncta.

(J) Quantification of large 33mer-containing puncta in the presence (F) and absence of exogenously added α_2M. For wide views of all panels in this figure, see Figure S3. Measurements done in triplicate (n = 3) different wells. Blue staining is DAPI, green staining is α_2M, and red staining is Cy5-33mer.

fibronectin via this pathway implies that a range of high-affinity TG2 substrates can induce the association of α_2M and TG2.

LRP-1 is responsible for receptor-mediated endocytosis of ternary complexes

Low-density lipoprotein (LDL) receptor-related protein 1 (LRP-1, also known as α_2M receptor or CD91), a member of the LDL receptor family, is responsible for receptor-mediated endocytosis of α_2M. Although this receptor is expressed on the surface of a wide range of cell types within the body, α_2M endocytosis by LRP-1 is only triggered when α_2M undergoes a conformational change upon binding to protease or non-protease ligands.[41] We sought to establish whether endocytosis of the ternary α_2M-TG2-peptide complex was mediated by LRP-1. Indeed, an earlier report showed that fibronectin binding to TG2 leads to its endocytosis through an LRP-1 mediated pathway; however, those investigators did not investigate the intermediacy of α_2M in this process.[42] Verification of a receptor-mediated endocytic pathway was first derived via the use of pharmacologic inhibitors of clathrin-mediated endocytosis. In comparison with untreated NRK cells (Figure 4A), cells treated with methyl-β-cyclodextrin (MβCD; Figure 4B), Pitstop-2 (Figure 4C), or Dyno-4a (Figure 4D) showed strong inhibition of α_2M and peptide co-localization as large endocytic puncta.

To demonstrate that LRP-1 is the primary receptor for this pathway, a potent endogenous antagonist of α_2M binding to LRP-1, receptor associated protein (RAP),[43] was recombinantly expressed and purified, and NRK cells were treated with RAP (Figure 4E) prior to treatment with Cy5-33mer and α_2M. Stable RAP tightly binds LRP-1 at the same site as activated α_2M and triggers receptor-mediated endocytosis; however, it does not dissociate from LRP-1 in the lysosomal compartment, thus inhibiting the recycling of the receptor.[43] RAP addition fully ablated

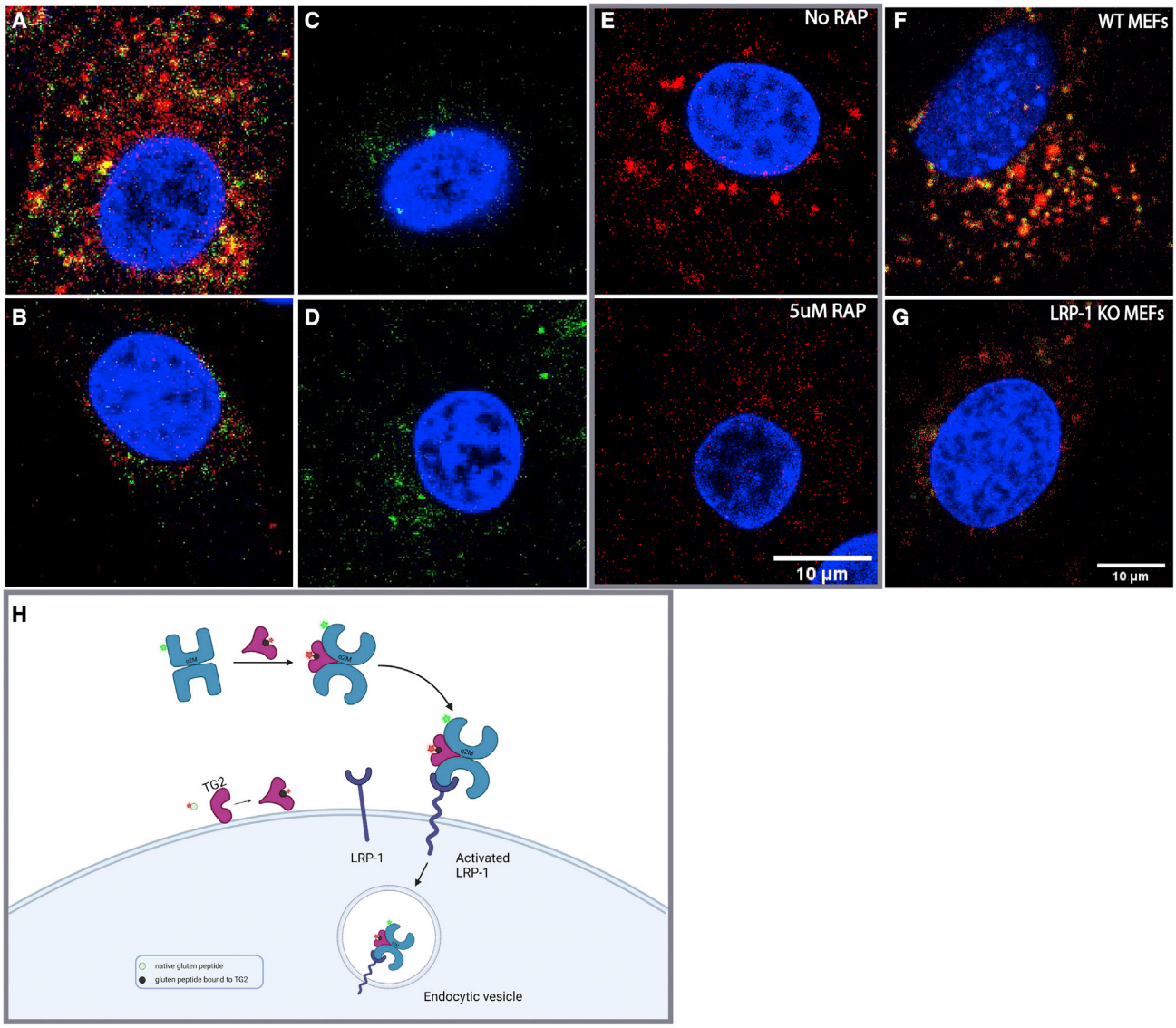

Figure 4. α_2M and 33mer endocytosis is clathrin dependent and involves the LRP-1 receptor

(A–D) Endocytosis of α_2M (green) and 33mer gluten peptide (red) by NRK cells. Inhibitors of clathrin-mediated endocytosis, including (B) 12.5 mM MβCD, (C) 20 μM Dyno-4a, or (D) 25 μM Pitstop abrogate the appearance of large puncta harboring both fluorescently labeled probes.

(E) The potent LRP-1 antagonist RAP inhibits the formation of large 33mer-containing puncta.

(F) Wild-type MEFs also readily internalize HB230 and a_2M in the presence of exogenous TRX and betamethasone.

(G) Under the same conditions, LRP-1 knockout MEFs show markedly reduced uptake of either probe in the form of large puncta. α_2M and HB230 were used at concentrations of 100 μg/mL and 10 μM, respectively. For wide views of all panels in this figure, see Figure S5.

(H) Schematic of mechanism of LRP-1 mediated endocytosis of the ternary gluten/TG2/α_2M complex. The native peptide is shown in green, whereas the TG2/gluten intermediate is represented in black. Conjugated fluorophores are shown as green and red stars. Blue staining is DAPI, green staining is α_2M, and red staining is Cy5-33mer.

the formation of large puncta, providing additional evidence that TG2 and its substrates undergo LRP-1-mediated endocytosis. Previous studies[44] have shown that LDL-type receptors such as LRP-1 are preferentially sorted into late endosomes and lysosomes rather than early endosomes. This aligns with the localization of the TG2-substrate complex described in Figure 2D, offering further evidence that the observed endocytosis is LRP-1 mediated and that the complex is directly trafficked to the lysosome.

Genetic evidence for the role of LRP-1 in this receptor-mediated endocytic process was obtained by comparing wild-type MEFs with their LRP-1 knockout counterparts. Whereas wild-type MEFs internalized the ternary complex generated by the addition of HB230 and α_2M (Figure 4F), knockout MEFs showed a marked defect in their ability to form large co-stained puncta under the same conditions (Figure 4G). Overall, the following sequence of events can be proposed (Figure 4H): TG2 binds its substrate at or near the cell surface. The resulting covalent

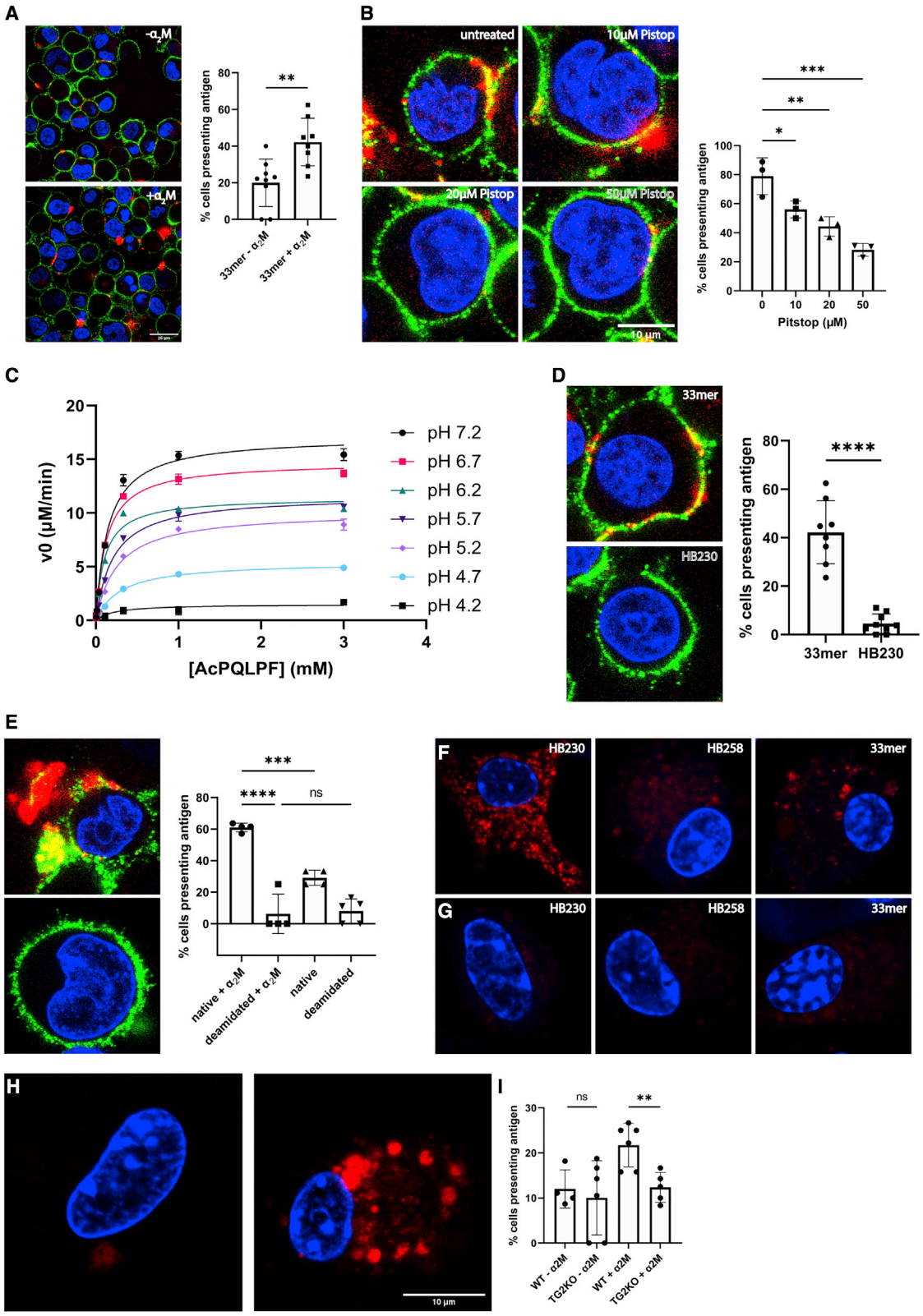

(legend on next page)

complex binds to α_2M, leading to LRP-1-mediated endocytosis of the ternary complex. Inside the endolysosomal compartment, the deamidated product of TG2 is released and made available for antigen presentation.

Relevance to CeD

To test the relevance of this novel lysosomal uptake pathway in the context of CeD, an EBV immortalized human B cell line (designated 9022) derived from an HLA-DQ2 homozygous individual was used.[45] In the presence of a low concentration (100 nM) of exogenously added recombinant human TG2, 9022 cells exposed to fluorescently labeled 33mer display this peptide in a class II MHC-restricted manner, as evidenced by a markedly clustered co-localization of HLA-DQ2 and the labeled 33mer on the surface of live cells (Figure 5A). Cell surface abundance of the labeled 33mer is enhanced upon addition of exogenous α_2M, implying that endocytosis precedes deamidative release of the gluten peptide from extracellular TG2. To confirm this, 9022 cells were treated with Pitstop for 20 min prior to addition of α_2M and 33mer. As expected, inhibition of clathrin-mediated endocytosis resulted in a dose-dependent reduction of cell surface 33mer labeling (Figure 5B). Direct evidence for the ability of the TG2-peptide thioester adduct to undergo endosomal turnover was obtained by evaluating the pH-dependence of TG2 activity. Under steady-state conditions, the catalytic activity of TG2 is preserved upon acidification until at least pH 5 (Figure 5C). The requirement of HLA-DQ2 for this dual surface labeling phenomenon was confirmed by verifying that HB230 did not localize to the cell surface under equivalent conditions (Figure 5D). The potency of this pathway for gluten antigen presentation is evident from a comparison of labeling intensity of the surface of 9022 cells in response to addition of equivalent concentrations of labeled 33mer or its deamidated analog. Although the latter peptide has higher affinity for HLA-DQ2,[46] stronger cell surface labeling was observed upon addition of the former peptide (Figure 5E), highlighting the power of the LRP-1 pathway defined in this study to concentrate low levels of gluten antigens while simultaneously delivering them to HLA-DQ2.

To verify the physiological relevance of the LRP-1 pathway for the uptake of TG2 substrates by professional APCs, bone marrow-derived dendritic cells (BMDCs) were isolated from wild-type (Figure 5F) or TG2-knockout (Figure 5G) mice. Both HB230 and Cy5-33mer were readily taken up by wild-type BMDCs, whereas neither probe was taken up by TG2-knockout BMDCs. Furthermore, significant cellular uptake of HB258 was not observed in either BMDC culture. Similarly, bone marrow-derived macrophages (BMM) also robustly internalized the 33mer in the presence, but not absence, of α_2M. Finally, TG2-knockout BMM did not show significant uptake of the 33mer (Figures 5H and 5I). These findings are consistent with the observed elevated expression of the *lrp1* gene in mouse dendritic cells and macrophages, but not B cells (Figure S6).

DISCUSSION

Celiac disease (CeD) is a widespread autoimmune disorder in which the primary environmental trigger, dietary gluten, supplies antigens that elicit an inflammatory response from disease-specific $CD4^+$ T cells. Two additional human proteins play essential roles in the pathogenic cascade.[7] Extracellular transglutaminase-2 (TG2) catalyzes sequence-specific deamidation of one or more Gln residues in antigenic gluten peptides, while HLA-DQ2 (or -DQ8) binds tightly to the resulting acidic (Glu-harboring) peptides, thereby enabling their presentation to T cell receptors. While the biochemical logic of these enzyme-substrate and ligand-receptor interactions are well understood, their physiological context remains to be defined. Specifically, given that small amounts of dietary gluten can trigger inflammation in CeD patients, a non-specific pinocytotic mechanism for antigen uptake and presentation (Figure 6A) is unlikely to achieve the requisite threshold for inducing pathogenic CD4 T cell responses.

The prevalent model for gluten antigen presentation to CeD-specific inflammatory T cells invokes a role for TG2-specific autoreactive B cells as the principal type of antigen-presenting cell (APC)[47] (Figure 6B). The elegance of this mechanism stems from three features: (1) the ability of these cells to take up TG2-bound gluten peptides via high-affinity interaction with their B cell receptors; (2) the ability of internalized gluten peptides to undergo deamidation (via the second half-reaction catalyzed by TG2; Figure 1A) and be presented to disease-specific T cell receptors in a DQ2/8-restricted manner; and (3) the ability of these mutually reinforcing B cell/T cell interactions to induce B cell maturation into plasmablasts capable of secreting anti-TG2 autoantibodies.

A major limitation of this model for gluten-mediated inflammation is that it cannot be readily extrapolated to professional APCs lacking a B cell receptor. To that end, our findings reported

Figure 5. HLA-DQ2 expressing B cells (9022) present gluten peptides on the cell surface in an α_2M-dependent manner

(A) In the presence of α_2M (right) the number of cells displaying gluten peptides on their surface increases compared with treating with peptide alone (left). The bar graph shows quantification over 150 cells from two to four frames of three to six experimental replicates, $^{**}p < 0.01$.

(B) Inhibition of clathrin-mediated endocytosis with the tool compound Pitstop decreases cell surface presentation of gluten peptides in a dose-dependent manner, $^{*}p < 0.05$, $^{**}p < 0.01$, $^{***}p < 0.001$.

(C) Steady-state kinetic analysis of TG2-catalyzed deamidation of Ac-PQLPF-NH_2 in response to increasing acidification in the pH 4.2–7.2 range. Measurements done in triplicate.

(D) The TG2 inhibitor HB230 is not recognized by HLA-DQ2, and therefore does not appear on the cell surface, $^{****}p < 0.0001$.

(E) Under conditions where the native 33mer strongly labels the cell surface (top), its deamidated analog is less active (bottom) despite that the latter peptide has higher affinity for HLA-DQ2. In all experiments, 9022 cells were treated with 100 nM recombinant TG2, $^{***}p < 0.001$, $^{****}p < 0.0001$.

(F) Bone marrow-derived dendritic cells (BMDCs) take up HB230 and 33mer, as previously described, whereas (G) no uptake is observed in BMDCs from TG2-knockout mice.

(H) Macrophages from TG2-knockout mice also do not internalize 33mer (left), whereas macrophages from wild-type mice show robust uptake in the presence of α_2M (right).

(I) Quantification of 33mer uptake in wild-type and TG2-knockout bone marrow-derived macrophages. Measurements done in triplicate, $^{**}p < 0.01$. For wide views of all panels in this figure, see Figure S6. Blue staining is DAPI, green staining is HLA-DQ2, and red staining is Cy5-33mer or HB230 as indicated. In all bar graphs, data are represented as mean ± SD.

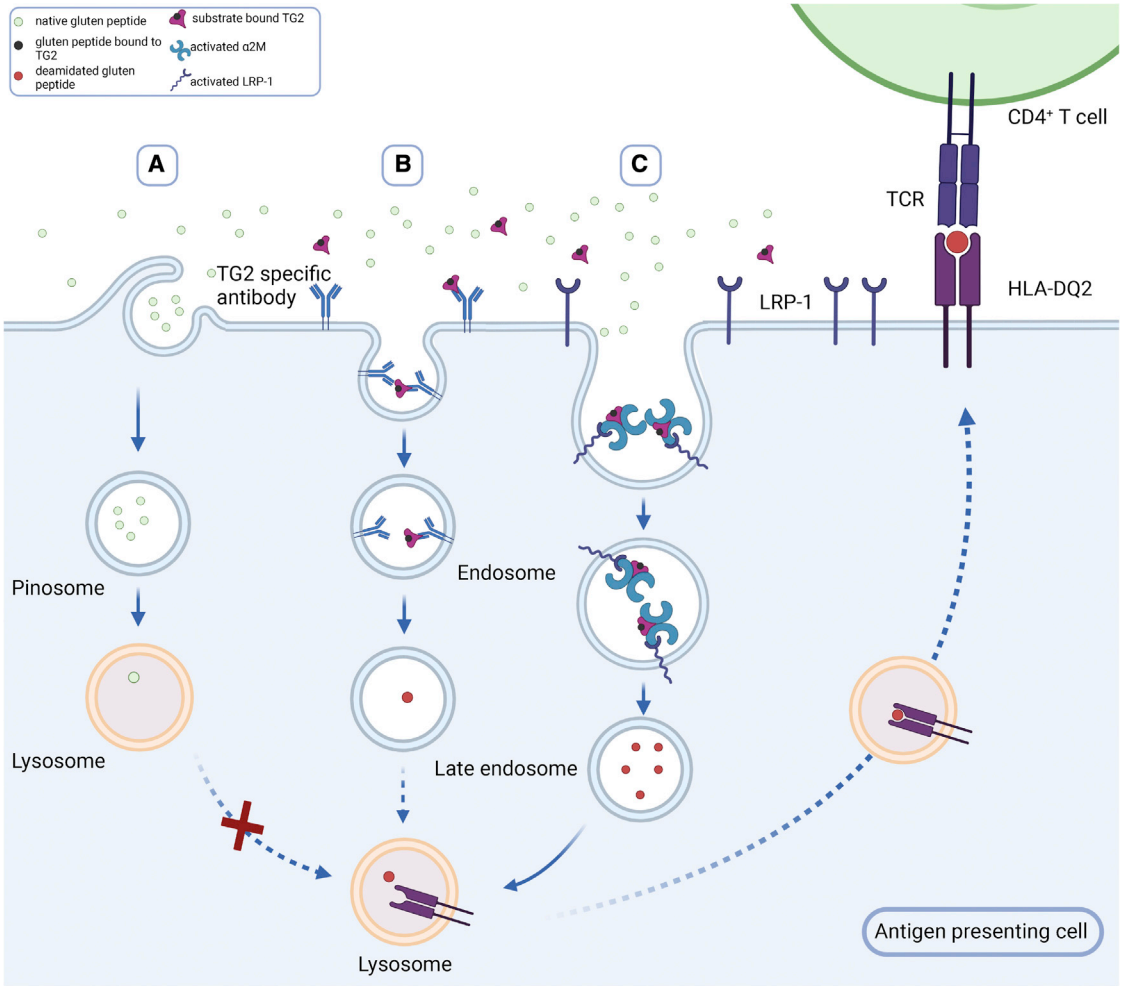

Figure 6. Alternative mechanisms for gluten antigen uptake and presentation in APCs

Given that small amounts of dietary gluten can induce inflammatory T cell activity in CeD patients, the typical concentrations of antigenic deamidated gluten peptides in the extracellular matrix is expected to be low.

(A) While pinocytosis may lead to some non-specific uptake of the native gluten peptides, it is unlikely to result in deamidated gluten peptide uptake and presentation above a requisite threshold.

(B) A prevalent model for gluten antigen presentation to CeD-specific inflammatory T cells invokes a role for TG2-specific autoreactive B cells as the principal type of antigen-presenting cell. In this model, B cells with autoreactive receptors recognize the acyl-enzyme intermediate formed between TG2 and an antigenic gluten peptide. This intermediate dissociates upon undergoing endocytosis, leading to lysosomal delivery and class II MHC presentation of deamidated gluten peptides by autoreactive B cells.

(C) Our studies have revealed a new mechanism for gluten antigen presentation wherein the ternary TG2-gluten-α2M complex undergoes potent LRP-1 dependent endocytosis. Subsequent endosomal release of the deamidated peptide also leads to class II MHC presentation; however, this pathway can operate in other professional antigen-presenting cells such as dendritic cells and macrophages.

in this study shine light on an unprecedented and potent pathway for gluten antigen presentation that likely operates in dendritic cells and/or macrophages of CeD patients (Figure 6C). Because this pathway involves recognition of some (but not all) TG2-gluten complexes by α_2-macroglobulin (α_2M), it selects the corresponding peptides as preferred sources of T cell antigens. In turn, the ternary complex undergoes LRP-1 mediated endocytosis. Two features of our proposed mechanism are especially noteworthy.

First, because LRP-1 is unable to engage free TG2 or α_2M, a vast fraction of each ubiquitous extracellular protein remains pathogenically inert. As such, this is a gluten-induced "gain-of-function" mechanism with respect to both TG2 and α_2M. Our data (Figure S4) suggest that the C-terminal β-barrel domain of TG2 plays a critical role in this interaction, although the domain of α_2M on which gluten-bound TG2 docks remains to be determined in further studies. Interestingly, others have reported that TG2 can bind to LRP-1 without the intermediacy of α_2M.[42] However, due to the abundance of α_2M in serum-containing cell culture media, the functional implications of constitutive TG2-LRP-1 interactions are unclear. Direct biochemical analyses are warranted to compare the physical and functional characteristics of gluten peptide-induced TG2- α_2M-LRP-1 interactions with those of the interaction of LRP-1 with unliganded TG2.

Second, because LRP-1 is expressed on many but not all cells in the human body and is highly expressed in certain populations of macrophages and dendritic cells (Figure S7), this pathway has the potential to internalize antigenic gluten peptides in APCs endowed with both LRP-1 and catalytically active TG2 on their surfaces. Indeed, our fluorescent molecular probe HB230 offers a direct glimpse into the potency of this receptor-mediated endocytosis pathway for antigen uptake relative to constitutive micropinocytosis, which engulfs soluble extracellular macromolecules through small vesicles and presumably corresponds to the small puncta in Figure 2. Further definition of cell types in the celiac and control intestine that display robust surface TG2 activity as well as LRP-1-mediated endocytosis activity is expected to be important for fully understanding the implications of this pathway in the onset and persistence of celiac disease. Other examples of potent receptor-mediated endocytic processes for antigen uptake by professional APCs include those mediated by C-type lectin receptors of dendritic cells such as the mannose receptor,[48,49] langerin,[50] and DEC205.[51]

The evolutionary logic of this new receptor-mediated endocytic pathway for antigen presentation remains to be explored. Previous studies have shown the role of LRP-1 in complex with receptor tyrosine kinase AXL and Ran-binding protein 9 in cross presentation by promoting efforocytosis.[52] Here we show that by taking advantage of forming a complex with two other ubiquitous extracellular proteins, TG2 and α_2M, LRP-1 offers a *covalent* ligation strategy for a variety of self and non-self substrates of TG2 to be removed from the extracellular environment of a range of cells. In the case of gluten peptides in CeD patients, the TG2 substrates then progress to be presented to T cells in a class II MHC-restricted manner. We speculate that the evolutionary origins of this pathway lie in processes that play a critical role in extracellular matrix remodeling, but that it has been coopted for antigen presentation by LRP-1-expressing APCs. Interestingly, extracellular proteins associated with neurodegenerative diseases have been identified as TG2 substrates.[53] For example, the microtubule-associated protein tau, which has a central role in several forms of dementias known as taupathies,[54] is a TG2 substrate[55] and has also been shown to undergo LRP-1-dependent endocytosis.[56] As such, the pathogenic role of this pathway may extend beyond CeD.

Limitations of the study

While the kinetic data presented here support an allosteric interaction between alpha-2-macroglobulin (α_2M) and transglutaminase-2 (TG2), our data fall short of providing physical evidence for direct binding between these two proteins. Preliminary efforts to detect this protein-protein interaction through bio-layer interferometry have proven unsuccessful, and further efforts are warranted using complementary methods.

Significance

While the environmental and genetic factors necessary for celiac disease pathogenesis are well defined, the mechanisms for gluten antigen processing have not been well characterized. In order to reach a pathogenic threshold, gluten peptides must be concentrated in the lysosome prior to DQ2-restricted MHC-II presentation. Here we describe a potent mechanism for lysosomal concentration of deamidated gluten peptides based on highly specific protein-protein interactions among three widely expressed proteins, transglutaminase-2, α_2M, and LRP-1. Since this pathway is active in many cell types, our work invokes a pathogenic role for dendritic cells and macrophages as APCs in the context of celiac disease. This pathway also leads to efficient lysosomal clearance of transglutaminase-2 substrates, several of which are disease associated, pointing toward a role for transglutaminase-2 in the pathogenesis of diseases beyond celiac disease.

STAR★METHODS

Detailed methods are provided in the online version of this paper and include the following:

- KEY RESOURCES TABLE
- RESOURCE AVAILABILITY
  - Lead contact
  - Materials availability
  - Data and code availability
- EXPERIMENTAL MODEL AND SUBJECT DETAILS
  - Cells and reagents
- METHOD DETAILS
  - Synthesis of inhibitors
  - General peptide synthesis protocol
  - Preparation of recombinant human thioredoxin (TRX)
  - Preparation of recombinant human transglutaminase 2 (TG2)
  - Preparation of recombinant human α_2-macroglobulin (α_2M) from mammalian cells
  - Preparation of recombinant human receptor associated protein (RAP)
  - Kinetic assays
  - Cell culture
  - Generation of MEF$^{-/-}$cell line
  - Conjugation α_2M with an NHS-linked fluorophore
  - Cellular assays – Adherent cells
  - Generation of NRK RFP-LAMP-1 cell line
  - Cellular assays – Suspension cells
  - Isolation and differentiation of BMDC and BMM
  - Confocal immunofluorescent microscopy
- QUANTIFICATION AND STATISTICAL ANALYSIS
  - Calculation of kinetic parameters
  - Colocalization analysis
  - HB230-containing vesicles quantification in NRK cells
  - Quantification of antigen presentation by 9022 cells
  - Statistical analysis

SUPPLEMENTAL INFORMATION

Supplemental information can be found online at https://doi.org/10.1016/j.chembiol.2022.12.002.

ACKNOWLEDGMENTS

This work was supported by a grant from the NIH (R01 DK063158 to C.K. and B.J.). H.A.B was supported by the NIH (F30DK132903) and the Stanford University Medical Scientist Training Program (T32GM007365 and T32GM145402). The authors thank Uche Medoh and Dr. Monther Abu-Remaileh for providing the RFP-LAMP-1 lentivirus construct, and Dr. Satyajit Mayor for helpful feedback on the manuscript.

AUTHOR CONTRIBUTIONS

E.L. and C.K. conceived the study. E.L. performed cell assays, and collected and analyzed data. H.B. and C.K. designed, synthesized, and validated HB230, HB225, Cy5-33mer, and other chemical probes. A.S.S. performed interaction assays involving α_2M and wild-type TG2 as well as its truncated derivatives. F.C.Y. performed *ex vivo* experiments. B.J. provided guidance on assay design and developing the manuscript's narrative. E.L. and C.K. wrote the manuscript with input from all authors.

DECLARATION OF INTERESTS

C.K. serves as a consultant to GSK and ImmunogenX. A patent application has been filed by Stanford University based on aspects of this work.

Received: July 25, 2022
Revised: October 17, 2022
Accepted: December 15, 2022
Published: January 5, 2023

REFERENCES

1. Lionetti, E., Gatti, S., Pulvirenti, A., and Catassi, C. (2015). Celiac disease from a global perspective. Best Pract. Res. Clin. Gastroenterol. *29*, 365–379. https://doi.org/10.1016/j.bpg.2015.05.004.
2. Leffler, D.A., Green, P.H.R., and Fasano, A. (2015). Extraintestinal manifestations of coeliac disease. Nat. Rev. Gastroenterol. Hepatol. *12*, 561–571. https://doi.org/10.1038/nrgastro.2015.131.
3. Sollid, L.M., and Jabri, B. (2013). Triggers and drivers of autoimmunity: lessons from coeliac disease. Nat. Rev. Immunol. *13*, 294–302. https://doi.org/10.1038/nri3407.
4. Rubin, J.E., and Crowe, S.E. (2020). Celiac disease. Ann. Intern. Med. *172*, ITC1–ITC16. https://doi.org/10.7326/aitc202001070.
5. Pinkas, D.M., Strop, P., Brunger, A.T., and Khosla, C. (2007). Transglutaminase 2 undergoes a large conformational change upon activation. PLoS Biol. *5*, e327. https://doi.org/10.1371/journal.pbio.0050327.
6. Plugis, N.M., Palanski, B.A., Weng, C.H., Albertelli, M., and Khosla, C. (2017). Thioredoxin-1 selectively activates transglutaminase 2 in the extracellular matrix of the small intestine: implications for celiac disease. J. Biol. Chem. *292*, 2000–2008. https://doi.org/10.1074/jbc.M116.767988.
7. Sollid, L.M. (2017). The roles of MHC class II genes and post-translational modification in celiac disease. Immunogenetics *69*, 605–616. https://doi.org/10.1007/s00251-017-0985-7.
8. Abadie, V., Kim, S.M., Lejeune, T., Palanski, B.A., Ernest, J.D., Tastet, O., Voisine, J., Discepolo, V., Marietta, E.v., Hawash, M.B.F., et al. (2020). IL-15, gluten and HLA-DQ8 drive tissue destruction in coeliac disease. Nature *578*, 600–604. https://doi.org/10.1038/s41586-020-2003-8.
9. Shan, L., Molberg, Ø., Parrot, I., Hausch, F., Filiz, F., Gray, G.M., Sollid, L.M., and Khosla, C. (2002). Structural basis for gluten intolerance in celiac sprue. Science *297*, 2275–2279. https://doi.org/10.1126/science.1074129.
10. Kim, C.-Y., Quarsten, H., Bergseng, E., Khosla, C., and Sollid, L.M. (2004). Structural basis for HLA-DQ2-mediated presentation of gluten epitopes in celiac disease. Proc. Natl. Acad. Sci. USA *101*, 4175–4179. https://doi.org/10.1073/pnas.0306885101.
11. Qiao, S.-W., Bergseng, E., Molberg, Ø., Xia, J., Fleckenstein, B., Khosla, C., and Sollid, L.M. (2004). Antigen presentation to celiac lesion-derived T cells of a 33-mer gliadin peptide naturally formed by gastrointestinal digestion. J. Immunol. *173*, 1757–1762. https://doi.org/10.4049/jimmunol.173.3.1757.
12. Vader, W., Stepniak, D., Kooy, Y., Mearin, L., Thompson, A., van Rood, J.J., Spaenij, L., and Koning, F. (2003). The HLA-DQ2 gene dose effect in celiac disease is directly related to the magnitude and breadth of gluten-specific T cell responses. Proc. Natl. Acad. Sci. USA *100*, 12390–12395. https://doi.org/10.1073/pnas.2135229100.
13. Jabri, B., and Sollid, L.M. (2009). Tissue-mediated control of immunopathology in coeliac disease. Nat. Rev. Immunol. *9*, 858–870. https://doi.org/10.1038/nri2670.
14. Trombetta, E.S., and Mellman, I. (2005). Cell biology of antigen processing in vitro and in vivo. Annu. Rev. Immunol. *23*, 975–1028. https://doi.org/10.1146/annurev.immunol.22.012703.104538.
15. Ráki, M., Tollefsen, S., Molberg, Ø., Lundin, K.E.A., Sollid, L.M., and Jahnsen, F.L. (2006). A unique dendritic cell subset accumulates in the celiac lesion and efficiently activates gluten-reactive T cells. Gastroenterology *131*, 428–438. https://doi.org/10.1053/j.gastro.2006.06.002.
16. di Sabatino, A., Pickard, K.M., Gordon, J.N., Salvati, V., Mazzarella, G., Beattie, R.M., Vossenkaemper, A., Rovedatti, L., Leakey, N.A.B., Croft, N.M., et al. (2007). Evidence for the role of interferon-alfa production by dendritic cells in the Th1 response in celiac disease. Gastroenterology *133*, 1175–1187. https://doi.org/10.1053/j.gastro.2007.08.018.
17. Hudec, M., Riegerová, K., Pala, J., Kútna, V., Černá, M., and ÓLeary, V.B. (2021). Celiac disease defined by over-sensitivity to gliadin activation and superior antigen presentation of dendritic cells. Int. J. Mol. Sci. *22*, 9982. https://doi.org/10.3390/ijms22189982.
18. Arranz, E., De Prado, Á., Fiz-López, A., Arribas, E., Garrote, J.A., and Bernardo, D. (2021). Human intestinal dendritic cell and macrophage subsets in coeliac disease. Int. Rev. Cell Mol. Biol. *358*, 85–104. https://doi.org/10.1016/BS.IRCMB.2020.09.006.
19. Neutra, M.R., Pringault, E., and Kraehenbuhl, J.-P. (1996). Antigen sampling across epithelial barriers and induction of mucosal immune responses. Annu. Rev. Immunol. *14*, 275–300. https://doi.org/10.1146/annurev.immunol.14.1.275.
20. Siegel, M., Strnad, P., Watts, R.E., Choi, K., Jabri, B., Omary, M.B., and Khosla, C. (2008). Extracellular transglutaminase 2 is catalytically inactive, but is transiently activated upon tissue injury. PLoS One *3*, e1861. https://doi.org/10.1371/journal.pone.0001861.
21. Klöck, C., DiRaimondo, T.R., and Khosla, C. (2012). Role of transglutaminase 2 in celiac disease pathogenesis. Semin. Immunopathol. *34*, 513–522. https://doi.org/10.1007/s00281-012-0305-0.
22. Zhuang, R., and Khosla, C. (2020). Substrates, inhibitors, and probes of mammalian transglutaminase 2. Anal. Biochem. *591*, 113560. https://doi.org/10.1016/j.ab.2019.113560.
23. Jeon, W.M., Lee, K.N., Birckbichler, P.J., Conway, E., and Patterson, M.K. (1989). Colorimetric assay for cellular transglutaminase. Anal. Biochem. *182*, 170–175. https://doi.org/10.1016/0003-2697(89)90737-9.
24. DiRaimondo, T.R., Klöck, C., Warburton, R., Herrera, Z., Penumatsa, K., Toksoz, D., Hill, N., Khosla, C., and Fanburg, B. (2014). Elevated transglutaminase 2 activity is associated with hypoxia-induced experimental pulmonary hypertension in mice. ACS Chem. Biol. *9*, 266–275. https://doi.org/10.1021/cb4006408.
25. Klöck, C., Herrera, Z., Albertelli, M., and Khosla, C. (2014). Discovery of potent and specific dihydroisoxazole inhibitors of human transglutaminase 2. J. Med. Chem. *57*, 9042–9064. https://doi.org/10.1021/jm501145a.
26. Levitzki, A., Willingham, M., and Pastan, I. (1980). Evidence for participation of transglutaminase in receptor-mediated endocytosis. Proc. Natl. Acad. Sci. USA *77*, 2706–2710. https://doi.org/10.1073/pnas.77.5.2706.
27. Davies, P.J., Davies, D.R., Levitzki, A., Maxfield, F.R., Milhaud, P., Willingham, M.C., and Pastan, I.H. (1980). Transglutaminase is essential in receptor-mediated endocytosis of α2-macroglobulin and polypeptide hormones. Nature *283*, 162–167. https://doi.org/10.1038/283162a0.
28. Vandooren, J., and Itoh, Y. (2021). Alpha-2-Macroglobulin in inflammation, immunity and infections. Front. Immunol. *12*, 803244. https://doi.org/10.3389/fimmu.2021.803244.
29. Mikhailenko, I., Battey, F.D., Migliorini, M., Ruiz, J.F., Argraves, K., Moayeri, M., and Strickland, D.K. (2001). Recognition of α2-macroglobulin by the low density lipoprotein receptor-related protein requires the cooperation of two ligand binding cluster regions. J. Biol. Chem. *276*, 39484–39491. https://doi.org/10.1074/jbc.m104382200.

30. Ganrot, P.O., and Scherstén, B. (1967). Serum α2-macroglobulin concentration and its variation with age and sex. Clin. Chim. Acta *15*, 113–120. https://doi.org/10.1016/0009-8981(67)90333-6.

31. Roche, P.A., and Furuta, K. (2015). The ins and outs of MHC class II-mediated antigen processing and presentation. Nat. Rev. Immunol. *15*, 203–216. https://doi.org/10.1038/nri3818.

32. Stamnaes, J., Pinkas, D.M., Fleckenstein, B., Khosla, C., and Sollid, L.M. (2010). Redox regulation of transglutaminase 2 activity. J. Biol. Chem. *285*, 25402–25409. https://doi.org/10.1074/jbc.m109.097162.

33. Yi, M.C., Melkonian, A. v, Ousey, J.A., and Khosla, C. (2018). Endoplasmic reticulum–resident protein 57 (ERp57) oxidatively inactivates human transglutaminase 2. J. Biol. Chem. *293*, 2640–2649. https://doi.org/10.1074/jbc.ra117.001382.

34. Melkonian, A. v, Loppinet, E., Martin, R., Porteus, M., and Khosla, C. (2021). An unusual "OR" gate for allosteric regulation of mammalian transglutaminase 2 in the extracellular matrix. J. Am. Chem. Soc. *143*, 10537–10540. https://doi.org/10.1021/jacs.1c04616.

35. Király, R., Csősz, É., Kurtán, T., Antus, S., Szigeti, K., Simon-Vecsei, Z., Korponay-Szabó, I.R., Keresztessy, Z., and Fésüs, L. (2009). Functional significance of five noncanonical Ca2+-binding sites of human transglutaminase 2 characterized by site-directed mutagenesis. FEBS J. *276*, 7083–7096. https://doi.org/10.1111/j.1742-4658.2009.07420.x.

36. Palanski, B.A., and Khosla, C. (2018). Cystamine and disulfiram inhibit human transglutaminase 2 via an oxidative mechanism. Biochemistry *57*, 3359–3363. https://doi.org/10.1021/acs.biochem.8b00204.

37. Hnida, K., Stamnaes, J., du Pré, M.F., Mysling, S., Jørgensen, T.J.D., Sollid, L.M., and Iversen, R. (2016). Epitope-dependent functional effects of celiac disease autoantibodies on transglutaminase 2. J. Biol. Chem. *291*, 25542–25552. https://doi.org/10.1074/jbc.m116.738161.

38. Liu, S., Cerione, R.A., and Clardy, J. (2002). Structural basis for the guanine nucleotide-binding activity of tissue transglutaminase and its regulation of transamidation activity. Proc. Natl. Acad. Sci. USA *99*, 2743–2747. https://doi.org/10.1073/pnas.042454899.

39. Soluri, M.F., Boccafoschi, F., Cotella, D., Moro, L., Forestieri, G., Autiero, I., Cavallo, L., Oliva, R., Griffin, M., Wang, Z., et al. (2019). Mapping the minimum domain of the fibronectin binding site on transglutaminase 2 (TG2) and its importance in mediating signaling, adhesion, and migration in TG2-expressing cells. FASEB J. *33*, 2327–2342. https://doi.org/10.1096/fj.201800054rrr.

40. Sima, L.E., Yakubov, B., Zhang, S., Condello, S., Grigorescu, A.A., Nwani, N.G., Chen, L., Schiltz, G.E., Arvanitis, C., Zhang, Z.-Y., et al. (2019). Small molecules target the interaction between tissue transglutaminase and fibronectin. Mol. Cancer Ther. *18*, 1057–1068. https://doi.org/10.1158/1535-7163.mct-18-1148.

41. Bres, E.E., and Faissner, A. (2019). Low density receptor-related protein 1 interactions with the extracellular matrix: more than meets the eye. Front. Cell Dev. Biol. *7*, 31. https://doi.org/10.3389/fcell.2019.00031.

42. Zemskov, E.A., Mikhailenko, I., Strickland, D.K., and Belkin, A.M. (2007). Cell-surface transglutaminase undergoes internalization and lysosomal degradation: an essential role for LRP1. J. Cell Sci. *120*, 3188–3199. https://doi.org/10.1242/jcs.010397.

43. Prasad, J.M., Migliorini, M., Galisteo, R., and Strickland, D.K. (2015). Generation of a potent low density lipoprotein receptor-related protein 1 (LRP1) antagonist by engineering a stable form of the receptor-associated protein (RAP) D3 domain. J. Biol. Chem. *290*, 17262–17268. https://doi.org/10.1074/jbc.M115.660084.

44. Lakadamyali, M., Rust, M.J., and Zhuang, X. (2006). Ligands for clathrin-mediated endocytosis are differentially sorted into distinct populations of early endosomes. Cell *124*, 997–1009. https://doi.org/10.1016/j.cell.2005.12.038.

45. Shiina, T., Ota, M., Shimizu, S., Katsuyama, Y., Hashimoto, N., Takasu, M., Anzai, T., Kulski, J.K., Kikkawa, E., Naruse, T., et al. (2006). Rapid evolution of major histocompatibility complex class I genes in primates generates new disease alleles in humans via hitchhiking diversity. Genetics *173*, 1555–1570. https://doi.org/10.1534/genetics.106.057034.

46. Xia, J., Sollid, L.M., and Khosla, C. (2005). Equilibrium and kinetic analysis of the unusual binding behavior of a highly immunogenic gluten peptide to HLA-DQ2. Biochemistry *44*, 4442–4449. https://doi.org/10.1021/bi047747c.

47. Iversen, R., Roy, B., Stamnaes, J., Høydahl, L.S., Hnida, K., Neumann, R.S., Korponay-Szabó, I.R., Lundin, K.E.A., and Sollid, L.M. (2019). Efficient T cell–B cell collaboration guides autoantibody epitope bias and onset of celiac disease. Proc. Natl. Acad. Sci. USA *116*, 15134–15139. https://doi.org/10.1073/pnas.1901561116.

48. Stahl, P.D., and Ezekowitz, R.A. (1998). The mannose receptor is a pattern recognition receptor involved in host defense. Curr. Opin. Immunol. *10*, 50–55. https://doi.org/10.1016/s0952-7915(98)80031-9.

49. Zehner, M., Chasan, A.I., Schuette, V., Embgenbroich, M., Quast, T., Kolanus, W., and Burgdorf, S. (2011). Mannose receptor polyubiquitination regulates endosomal recruitment of p97 and cytosolic antigen translocation for cross-presentation. Proc. Natl. Acad. Sci. USA *108*, 9933–9938. https://doi.org/10.1073/pnas.1102397108.

50. Ng, W.C., Londrigan, S.L., Nasr, N., Cunningham, A.L., Turville, S., Brooks, A.G., and Reading, P.C. (2016). The C-type lectin langerin functions as a receptor for attachment and infectious entry of influenza A virus. J. Virol. *90*, 206–221. https://doi.org/10.1128/jvi.01447-15.

51. Gully, B.S., Venugopal, H., Fulcher, A.J., Fu, Z., Li, J., Deuss, F.A., Llerena, C., Heath, W.R., Lahoud, M.H., Caminschi, I., et al. (2021). The cryo-EM structure of the endocytic receptor DEC-205. J. Biol. Chem. *296*, 100127. https://doi.org/10.1074/jbc.ra120.016451.

52. Subramanian, M., Hayes, C.D., Thome, J.J., Thorp, E., Matsushima, G.K., Herz, J., Farber, D.L., Liu, K., Lakshmana, M., and Tabas, I. (2014). An AXL/LRP-1/RANBP9 complex mediates DC efferocytosis and antigen cross-presentation in vivo. J. Clin. Invest. *124*, 1296–1308. https://doi.org/10.1172/JCI72051.

53. Min, B., and Chung, K.C. (2018). New insight into transglutaminase 2 and link to neurodegenerative diseases. BMB Rep. *51*, 5–13. https://doi.org/10.5483/bmbrep.2018.51.1.227.

54. Kovacs, G.G. (2017). Tauopathies. Handb. Clin Neurol. *145*, 355–368. https://doi.org/10.1016/B978-0-12-802395-2.00025-0.

55. Halverson, R.A., Lewis, J., Frausto, S., Hutton, M., and Muma, N.A. (2005). Tau protein is cross-linked by transglutaminase in P301L tau transgenic mice. J. Neurosci. *25*, 1226–1233. https://doi.org/10.1523/jneurosci.3263-04.2005.

56. Rauch, J.N., Luna, G., Guzman, E., Audouard, M., Challis, C., Sibih, Y.E., Leshuk, C., Hernandez, I., Wegmann, S., Hyman, B.T., et al. (2020). LRP1 is a master regulator of tau uptake and spread. Nature *580*, 381–385. https://doi.org/10.1038/s41586-020-2156-5.

57. de Laurenzi, V., and Melino, G. (2001). Gene disruption of tissue transglutaminase. Mol. Cell Biol. *21*, 148–155. https://doi.org/10.1128/mcb.21.1.148-155.2001.

58. Piper, J.L., Gray, G.M., and Khosla, C. (2002). High selectivity of human tissue transglutaminase for immunoactive gliadin peptides: implications for celiac sprue. Biochemistry *41*, 386–393. https://doi.org/10.1021/bi011715x.

59. Hausch, F., Halttunen, T., Mäki, M., and Khosla, C. (2003). Design, synthesis, and evaluation of gluten peptide analogs as selective inhibitors of human tissue transglutaminase. Chem. Biol. *10*, 225–231. https://doi.org/10.1016/s1074-5521(03)00045-0.

60. Birsoy, K., Wang, T., Chen, W.W., Freinkman, E., Abu-Remaileh, M., and Sabatini, D.M. (2015). An essential role of the mitochondrial electron transport chain in cell proliferation is to enable aspartate synthesis. Cell *162*, 540–551. https://doi.org/10.1016/j.cell.2015.07.016.

STAR★METHODS

KEY RESOURCES TABLE

REAGENT or RESOURCE	SOURCE	IDENTIFIER
Antibodies		
α-transglutaminase 2 polyclonal antibody (raised in rabbit)	Custom made by Pacific Immunology	N/A
Chemicals, peptides, and recombinant proteins		
Recombinant transglutaminase 2	This paper	N/A
Alpha-2 macroglobulin (from plasma)	Athens Research and Technology	Cat #: 16-16-012013
Alpha-2 macroglobulin (recombinant)	This paper	N/A
HB230	This paper	N/A
HB225	This paper	N/A
Cy5-33mer (native)	This paper	N/A
Cy5-33mer (deamidated)	This paper	N/A
Experimental models: Cell lines		
Rat: Normal Rat Kidney Cells	ATCC	Cat #: CRL-6509
Mouse: LRP-1 knock-out MEFs	ATCC	Cat #: CRL-2216
Mouse: TG2 knock-out MEFs	Generated from TG2 KO mice	N/A
Mouse: MEF	Generated from wild type mice	N/A
Human male: 9022 B cells	International Histocompatibility Workshop	https://www.fredhutch.org/en/research/institutes-networks-ircs/international-histocompatibility-working-group.html
Experimental models: Organisms/strains		
TG2 knockout mice	De Laurenzi and Melino[57]	N/A
Recombinant DNA		
TG2 plasmid (in pET vector)	Palanski and Khosla[36]	pBAP3
Alpha-2 Macroglobulin	This paper	pASS1
RAP	This paper	RAP-pET21
Software and algorithms		
Fiji (ImageJ)	NIH	https://imagej.nih.gov/ij/download.html; RRID: SCR_003070
GraphPad Prism 9	Dotmatics	https://www.graphpad.com/; RRID: SCR_002798
ChemDraw	Perkin Elmer Informatics	https://perkinelmerinformatics.com/products/research/chemdraw; RRID: SCR_016768

RESOURCE AVAILABILITY

Lead contact

Further information and requests for resources and reagents should be directed to and will be fulfilled by the lead contact, Chaitan Khosla (khosla@stanford.edu).

Materials availability

All of the materials that support the conclusions relevant to this manuscript are available upon reasonable request from the lead contact without restriction.

Data and code availability

All data reported in this paper will be shared by the lead contact upon request. This paper does not include original code.

Any additional information required to reanalyze the data reported in this paper is available from the lead contact upon request.

EXPERIMENTAL MODEL AND SUBJECT DETAILS

Cells and reagents

Cell lines

NRK (ATCC, CRL-6509). LRP-1 KO MEF (ATCC, CRL-2216). The sex of these cell lines is not listed by the vendor. 9022 cells are part of the reference table generated in the 10 th International Histocompatibility Workshop, and were generously shared with us by the Sollid lab at the University of Oslo. The were derived from a male patient.

Media

High Glucose DMEM (Corning, 10-017-CV), RPMI 1640 (Corning, 10-040-CV), Expi293 Expression Medium (Gibco, A1435101), OptiMEM (Gibco, 31985070).

Fetal Bovine Serum

BenchMark Fetal Bovine Serum (GeminiBio, 100-106-500)

Cell culture antibiotics

Penicillin-Streptomycin (Corning, 30-002-CI)

Assay materials

Half area 96-well plates (Greiner, 675,001)

Enzymes and proteins

Alpha-2 Macroglobulin (Athens Research and technology, 16-16-012013), Glutamate Dehydrogenase (BBI solutions), chicken egg-white lysozyme (Thermo-Fischer, 12,650-88-3).

Chemicals

All chemicals used are from Sigma-Aldrich or TCI with the following exceptions: Buffer components and LB granulated media (Fisher). IPTG (Gold Bio, I12481), Ni-NTA resin (Qiagen, 30,210), HiTrap Q HP anion exchange columns (GE Healthcare, 17,115,301), Sulfo-Cy5 (Lumiprobe, 63,320), Alexa Fluor 555-NHS Ester (Invitrogen, A20009), Super-Dex 200 SEC Column (Cytiva, 28-9909-44), ExpiFectamine 293 Transfection Kit (Gibco, A14525), HiTrap Chelating HP column (Cytiva, 17,040,801), Sephacryl S-400-HR (17,060,910).

METHOD DETAILS

Synthesis of inhibitors

Abbrreviated inhibitor synthesis route depicted in Scheme 1B.

9: To a solution of boc-L-glutamic acid 1-*tert*-butyl ester (2.565 g, 8.46 mmol, 1 equiv) in dry DCM (0.3 M) was added *N*-methyl morpholine (2.32 mL, 21.1 mmol, 2.5 equiv). The resulting solution was cooled to 0°C and isobutyl chloroformate (1.37 mL, 10.6 mmol, 1.25 equiv) was added dropwise. After 30 min, *N,O*-dimethylhydroxylamine hydrochloride (989 mg, 10.1 mmol, 1.2 equiv) was added in a single addition. The solution was allowed to come to room temperature and stir for 3 h. The reaction was diluted with DCM and quenched with 1 M HCl. The aqueous phase was extracted three times with DCM and the combined organic phase was washed once with saturated $NaHCO_3$ and dried over sodium sulfate. The solvent was removed *en vacuo* and the crude product was purified with column chromatography (45% ethyl acetate: hexanes, Rf = 0.40) to provide **9** as a colorless oil (2.74 g, 93% yield).

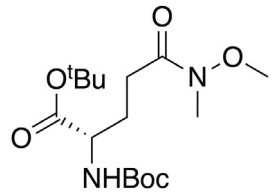

9

^{1}H NMR (400 MHz, $CDCl_3$) δ 5.19 (d, *J* = 8.3 Hz, 1H), 4.10 (h, *J* = 4.5 Hz, 1H), 3.60 (s, 3H), 3.09 (s, 3H), 2.54–2.34 (m, 2H), 2.13–2.00 (m, 1H), 1.85 (dtd, *J* = 14.2, 8.8, 6.0 Hz, 1H), 1.38 (s, 9H), 1.36 (s, 9H).

^{13}C NMR (101 MHz, $CDCl_3$) δ 173.50, 171.48, 155.41, 81.72, 79.38, 61.10, 53.68, 32.13, 28.22, 27.95, 27.88, 27.42.

HRMS (ESI) (*m/z*): calculated for $C_{16}H_{30}N_2O_6$ $[M + H]^+$: 347.2177, found: 347.2181.

10: To a solution of **9** (2.74 g, 7.90 mmol, 1 equiv) and DMAP (97 mg, 0.79 mmol, 0.1 equiv) in dry DCM (0.4 M) was added triethylamine (22 mL, 158 mmol, 20 equiv) and di-*tert*-butyl dicarbonate (9.1 mL, 39.5 mmol, 5 equiv). The solution was brought to reflux and allowed to stir for 3 h. The mixture was cooled to room temperature, diluted with DCM, and quenched with 1 M HCl. The aqueous phase was extracted three times with DCM. The combined organics were washed twice with 1 M HCl, dried over sodium sulfate,

and concentrated *en vacuo*. The crude product was purified by column chromatography (35% ethyl acetate: hexanes, Rf = 0.50) to provide 10 as a colorless oil (3.43 g, 97% yield).

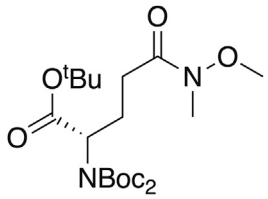

10

^{1}H NMR (400 MHz, $CDCl_3$) δ 4.83–4.67 (m, 1H), 3.62 (s, 3H), 3.12 (s, 3H), 2.57–2.33 (m, 3H), 2.17–2.02 (m, 1H), 1.46 (s, 18H), 1.40 (s, 9H).

^{13}C NMR (101 MHz, $CDCl_3$) δ 173.62, 169.41, 152.30, 82.76, 81.19, 61.14, 58.40, 32.20, 28.61, 27.99, 27.97, 24.36.

HRMS (ESI) (*m/z*): calculated for $C_{21}H_{38}N_2O_8$ [M + Na]$^+$: 469.2520, found: 469.2522.

11: To a solution of **10** (3.43 g, 7.68 mmol, 1 equiv) in dry THF (0.25 M) cooled to −78°C was added DIBAL-H (1 M in hexanes, 8.45 mL, 8.45 mmol, 1.1 equiv) dropwise. The solution was allowed to warm to room temperature and stir for 1 h. The reaction was quenched with 0.35 M $NaHSO_4$ and the aqueous phase was extracted twice with diethyl ether. The combined organics were washed twice with 1 N HCl, twice with saturated $NaHCO_3$, and twice with saturated NaCl. The solution was then dried over sodium sulfate and concentrated *en vacuo* to afford the crude aldehyde (2.93 g, 98% crude yield) which was used in the subsequent step without further purification.

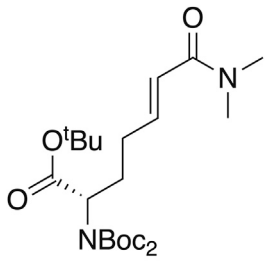

11

To a solution of **A** (2.02 g, 8.04 mmol, 1.05 equiv) in dry THF (0.4 M) was added potassium tert-butoxide (1 M in THF, 7.7 mL, 7.7 mmol, 1 equiv). The base was allowed to react for 30 min at room temperature after which the aldehyde dissolved in THF (20 mL) was added to the stirring ylide dropwise. The solution was allowed to stir for 1.5 h at room temperature. The reaction was diluted with ethyl acetate and quenched with saturated NH_4Cl. The aqueous phase was extracted twice with ethyl acetate and the combined organics were washed once with saturated NaCl, dried over sodium sulfate, and concentrated *en vacuo*. The crude product was purified by column chromatography (60% ethyl acetate: hexanes, Rf = 0.30) to provide the product as a colorless oil (2.74 g, 78% yield).

^{1}H NMR (400 MHz, $CDCl_3$) δ 6.83 (dt, *J* = 15.1, 6.6 Hz, 1H), 6.26 (dt, *J* = 15.1, 1.4 Hz, 1H), 4.75–4.65 (m, 1H), 3.04 (s, 3H), 2.97 (s, 3H), 2.29–2.13 (m, 3H), 2.07–1.94 (m, 1H), 1.48 (s, 18H), 1.42 (s, 9H).

^{13}C NMR (101 MHz, $CDCl_3$) δ 169.60, 166.73, 152.49, 144.52, 121.06, 82.93, 81.39, 58.39, 37.35, 35.70, 29.31, 28.08, 28.06, 27.98.

HRMS (ESI) (*m/z*): calculated for $C_{23}H_{40}N_2O_7$ [M + Na]$^+$: 479.2728, found: 479.2749.

12: To **11** (495 mg, 1.08 mmol, 1 equiv) was added 10 mL of a 1:1 mixture of trifluoroacetic acid and DCM. The solution was allowed to stir at room temperature for 2 h, after which the solvents were removed *en vacuo*. The resulting orange oil was taken up again in 10 mL of a 1:1 mixture of trifluoroacetic acid and DCM and allowed to stir for 2 h more at room temperature. After 4 h total, the solvents were removed *en vacuo* and the crude oil was taken up in 10 mL of DCM. The solution was cooled to 0°C after which DIPEA (755 μL, 4.34 mmol, 4 equiv) was added in a single addition. To the solution was added fmoc-*N*-hydroxy-succinimide ester (731 mg, 2.17 mmol, 2 equiv). The solution was warmed to room temperature and allowed to stir for 30 min. The reaction was quenched with 1 M HCl and extracted three times with DCM. The combined organics were washed twice with 1 M HCl and once with saturated NaCl, dried over sodium sulfate, and concentrated *en vacuo*. The crude product was purified by column chromatography (5% methanol: DCM +1% acetic acid, Rf = 0.32) to provide **12** as a white powder (403 mg, 88% yield).

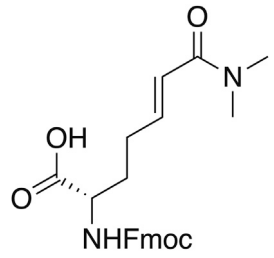

12

^{1}H NMR (500 MHz, DMSO) δ 12.65 (s, 1H), 7.90 (d, *J* = 7.5 Hz, 2H), 7.76–7.70 (m, 2H), 7.68 (d, *J* = 8.1 Hz, 1H), 7.42 (t, *J* = 7.4 Hz, 2H), 7.33 (td, *J* = 7.5, 1.2 Hz, 2H), 6.61 (dt, *J* = 15.1, 7.0 Hz, 1H), 6.38 (dt, *J* = 15.0, 1.5 Hz, 1H), 4.32–4.27 (m, 2H), 4.23 (t, *J* = 7.0 Hz, 1H), 3.94 (ddd, *J* = 9.9, 8.1, 4.4 Hz, 1H), 2.99 (s, 3H), 2.84 (s, 3H), 2.28–2.18 (m, 2H), 1.90–1.70 (m, 2H).

^{13}C NMR (126 MHz, DMSO) δ 173.73, 165.32, 156.14, 143.85, 143.77, 143.22, 140.73, 140.71, 127.64, 127.07, 125.26, 121.73, 120.13, 65.59, 53.09, 46.66, 36.66, 35.03, 29.56, 28.17.

HRMS (ESI) (*m/z*): calculated for $C_{24}H_{26}N_2O_5$ $[M + H]^+$: 423.1914, found: 423.1921.

13: A solution of **11** (237 mg, 0.52 mmol, 1 equiv) and cobalt (II) chloride hexahydrate in dry methanol (0.10 M) was cooled to 0°C. To the solution was added solid sodium borohydride (98 mg, 2.60 mmol, 5 equiv) in three additions. The solution was allowed to come to room temperature and stir for 30 min. The reaction was diluted with DCM and quenched with 1 N HCl. The aqueous layer was extracted three times with DCM and the combined organics were dried over sodium sulfate and concentrated. The crude product was purified by column chromatography (60% ethyl acetate: hexanes, Rf = 0.35) to afford **13** as a colorless oil (229 mg, 96% yield).

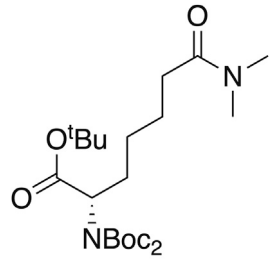

13

^{1}H NMR (400 MHz, $CDCl_3$) δ 4.68 (dd, *J* = 9.6, 5.2 Hz, 1H), 2.97 (s, 3H), 2.91 (s, 3H), 2.28 (t, *J* = 7.8 Hz, 2H), 2.12–1.98 (m, 1H), 1.84 (dtd, *J* = 14.2, 9.5, 6.4 Hz, 1H), 1.73–1.57 (m, 2H), 1.48 (s, 18H), 1.42 (s, 9H), 1.40–1.32 (m, 2H).

^{13}C NMR (101 MHz, $CDCl_3$) δ 172.94, 169.95, 152.53, 82.75, 81.15, 58.85, 37.31, 35.39, 33.26, 29.08, 28.07, 28.00, 26.36, 24.92.

HRMS (ESI) (*m/z*): calculated for $C_{23}H_{42}N_2O_7$ $[M + Na]^+$: 481.2884, found: 481.2908.

14: To **13** (300 mg, 0.65 mmol, 1 equiv) was added 6 mL of a 1:1 mixture of trifluoroacetic acid and DCM. The solution was allowed to stir at room temperature for 2 h, after which the solvents were removed *en vacuo*. The resulting orange oil was taken up again in 6 mL of a 1:1 mixture of trifluoroacetic acid and DCM and allowed to stir for 2 h more at room temperature. After 4 h total, the solvents were removed *en vacuo* and the crude oil was taken up in 6 mL of DCM. The solution was cooled to 0°C after which DIPEA (420 μL, 2.40 mmol, 4 equiv) was added in a single addition. To the solution was added fmoc-*N*-hydroxysuccinimide ester (441 mg, 1.31 mmol, 2 equiv). The solution was warmed to room temperature and allowed to stir for 30 min. The reaction was quenched with 1 M HCl and extracted three times with DCM. The combined organics were washed twice with 1 M HCl and once with saturated NaCl, dried over sodium sulfate, and concentrated *en vacuo*. The crude product was purified by column chromatography (5% methanol: DCM +1% acetic acid, Rf = 0.34) to provide **14** as a white powder (261 mg, 94% yield).

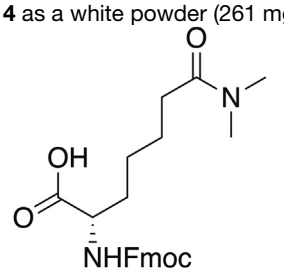

14

^{1}H NMR (500 MHz, DMSO) δ 12.57 (s, 1H), 7.89 (d, *J* = 7.6 Hz, 2H), 7.73 (d, *J* = 7.8 Hz, 2H), 7.63 (d, *J* = 8.2 Hz, 1H), 7.42 (t, *J* = 7.5 Hz, 2H), 7.33 (q, *J* = 7.1 Hz, 2H), 4.33–4.25 (m, 2H), 4.25–4.16 (m, 1H), 3.93 (ddd, *J* = 9.6, 8.2, 4.8 Hz, 1H), 2.93 (s, 3H), 2.79 (s, 3H), 2.26 (t, *J* = 7.5 Hz, 2H), 1.77–1.66 (m, 1H), 1.61 (dtd, *J* = 14.5, 9.5, 5.1 Hz, 1H), 1.55–1.41 (m, 2H), 1.41–1.27 (m, 2H).

^{13}C NMR (126 MHz, DMSO) δ 174.00, 171.79, 156.17, 143.84, 140.73, 127.64, 127.07, 125.31, 120.12, 65.60, 53.78, 46.67, 36.68, 34.77, 32.22, 30.69, 25.48, 24.22.

HRMS (ESI) (*m/z*): calculated for $C_{23}H_{42}N_2O_7$ [M + H]$^+$: 425.2071 found: 425.2078.

A: A 50 mL round-bottom flask was charged with triisopropyl phosphite (3.19 mL, 13.9 mmol, 1 equiv) and 2-bromo-*N,N*-dimethyl acetamide (1.50 mL, 13.9 mmol, 1 equiv). The flask was affixed with a condenser and heated in an oil bath to 130°C for 22 h. The reaction was cooled to room temperature and the crude product was purified directly by column chromatography (4% MeOH:DCM, Rf = 0.30) to give **A** as a pale yellow oil (2.34 g, 66% yield).

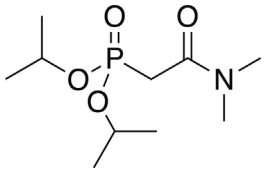

A

^{1}H NMR (500 MHz, $CDCl_3$) δ 4.64 (dhept, *J* = 7.9, 6.2 Hz, 2H), 3.02 (s, 3H), 2.90 (d, *J* = 22.3 Hz, 2H), 2.86 (d, *J* = 1.5 Hz, 3H), 1.23 (dd, *J* = 6.3, 3.4 Hz, 12H).

^{13}C NMR (126 MHz, $CDCl_3$) δ 164.87 (d, *J* = 5.7 Hz), 71.23 (d, *J* = 6.8 Hz), 38.50, 35.69, 34.55 (d, *J* = 133.9 Hz), 23.95 (d, *J* = 4.0 Hz), 23.77 (d, *J* = 5.1 Hz).

^{31}P NMR (202 MHz, $CDCl_3$) δ 19.25 (tt, *J* = 22.2, 7.8 Hz).

HRMS (ESI) (*m/z*): calculated for $C_{19}H_{22}NO_4P$ [M + H]$^+$: 252.1359 found: 252.1362.

General peptide synthesis protocol

Peptides were synthesized using standard Fmoc chemistry on a CSBio instrument. For peptides with C-terminal amides, Fmoc-Rink resin was used (CSBio), and for peptides with C-terminal acids, Wang resin with the appropriate C-terminal amino acid conjugated to it was used (Novabiochem). Synthesis was performed with 250 μmol of resin and 1 mmol of the Fmoc amino acids. Fmoc deprotection was carried out with 20% piperidine in DMF and coupling was performed using 1 mmol of HBTU over 1 h at room temperature. N-terminal acetylation was performed with 11 mL of 7:2:2 DMF:acetic anhydride:DIPEA (v/v/v) overnight at room temperature. Resins were dried over vacuum for 2 h before cleavage. Dry peptide resin was cleaved with 95% TFA, 2.5% H_2O, 2.5% triisopropylsilane over 3 h at room temperature. The cleavage cocktail was evaporated under a stream of nitrogen and the crude peptide was precipitated with cold diethyl ether. The precipitate was centrifuged (3500 g for 4 min), diethyl ether was decanted, and the crude solid was triturated twice more with cold diethyl ether. The resulting white solid was lyophilized from H_2O/ACN before purification with preparative RP-HPLC (A = H_2O + 0.1% TFA, B = ACN +0.1% TFA). The identity and purity of the fractions were confirmed by LCMS analysis and those corresponding to the peptide of interested were pooled and lyophilized.

1 (HB-225): 1 was synthesized using the general peptide synthesis protocol described above using Fmoc-Pro-OH, Fmoc-Leu-OH, Fmoc-Phe-OH, and 12. The crude peptide was purified by RP-HPLC (C18 preparative column, 35% B isocratic over 30 min) to yield a white solid (130 mg, 75% yield).

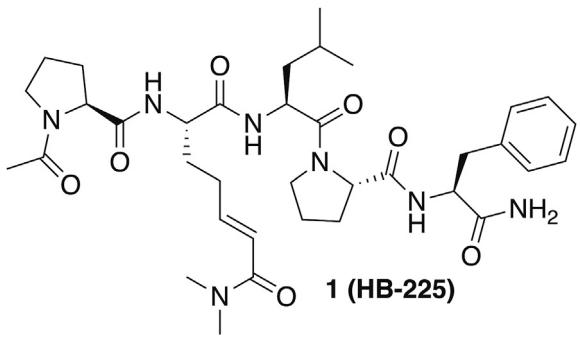

1 (HB-225)

HRMS (ESI) (*m/z*): calculated for $C_{36}H_{53}N_7O_7$ [M + H]$^+$: 696.4079 found: 696.4099.

15: **15** was synthesized using the general peptide synthesis protocol described above using Fmoc-Pro-OH, Fmoc-Dab(Boc)-OH, Fmoc-Phe-OH, and 12. After cleavage, the material was taken on to the next step without further purification.

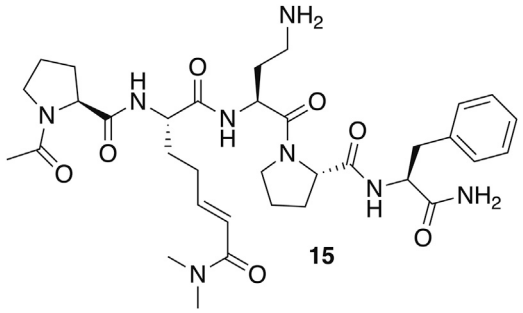

HRMS (ESI) (*m/z*): calculated for $C_{34}H_{50}N_8O_7$ $[M + H]^+$: 683.3875 found: 683.3890.

2 (HB-230): **15** (7.5 mg, 11.0 μmol, 1 equiv) was dissolved in 1 mL of 100 mM $NaHCO_3$ buffer (pH = 8.4). Solid SulfoCy5-*N*-hydroxysuccinimide ester (16.2 mg, 22.0 μmol, 2 equiv) was added. The solution was protected from light and allowed to stand overnight at room temperature. After 18 h, the crude mixture was lyophilized. The resulting crude solid was purified by RP-HPLC (C18 preparative column, 25% B to 40% B over 30 min). The appropriate fractions were combined and lyophilized to yield a blue solid (7.0 mg, 49% yield).

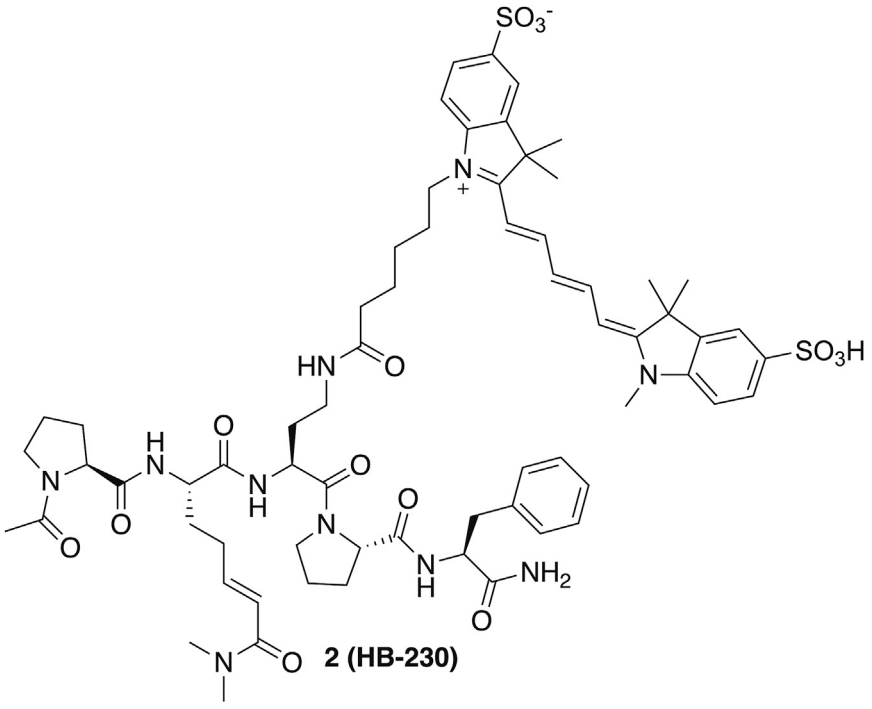

HRMS (ESI) (*m/z*): calculated for $C_{66}H_{86}N_{10}O_{14}S_2$ $[M+2H]^{2+}$: 654.2956 found: 654.2970.

16: HB-02-057 was synthesized using the general peptide synthesis protocol described above using Fmoc-Pro-OH, Fmoc-Dab(Boc)-OH, Fmoc-Phe-OH, and **14**. The crude peptide was purified by RP-HPLC (C18 preparative column, 25% B isocratic over 30 min) to yield a white solid (70 mg, 41% yield).

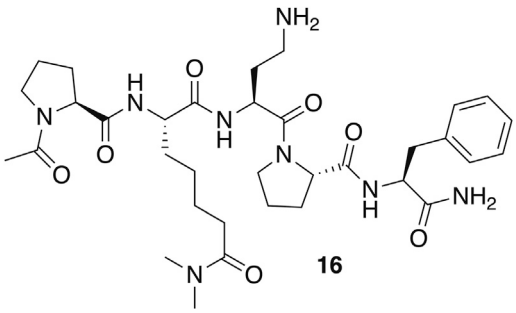

HRMS (ESI) (*m/z*): calculated for $C_{34}H_{52}N_8O_7$ $[M + H]^+$: 685.4032 found: 685.4055.

5 (HB-258): **16** (9.4 mg, 13.7 μmol, 1 equiv) was dissolved in 1 mL of 100 mM $NaHCO_3$ buffer (pH = 8.4). Solid SulfoCy5-*N*-hydroxysuccinimide ester (20.3 mg, 27.4 μmol, 2 equiv) was added. The solution was protected from light and allowed to stand overnight at room temperature. After 18 h, the crude mixture was lyophilized. The resulting crude solid was taken up purified by RP-HPLC (C18 preparative column, 25% B to 40% B over 30 min). The appropriate fractions were combined and lyophilized to yield a blue solid (9.0 mg, 50% yield).

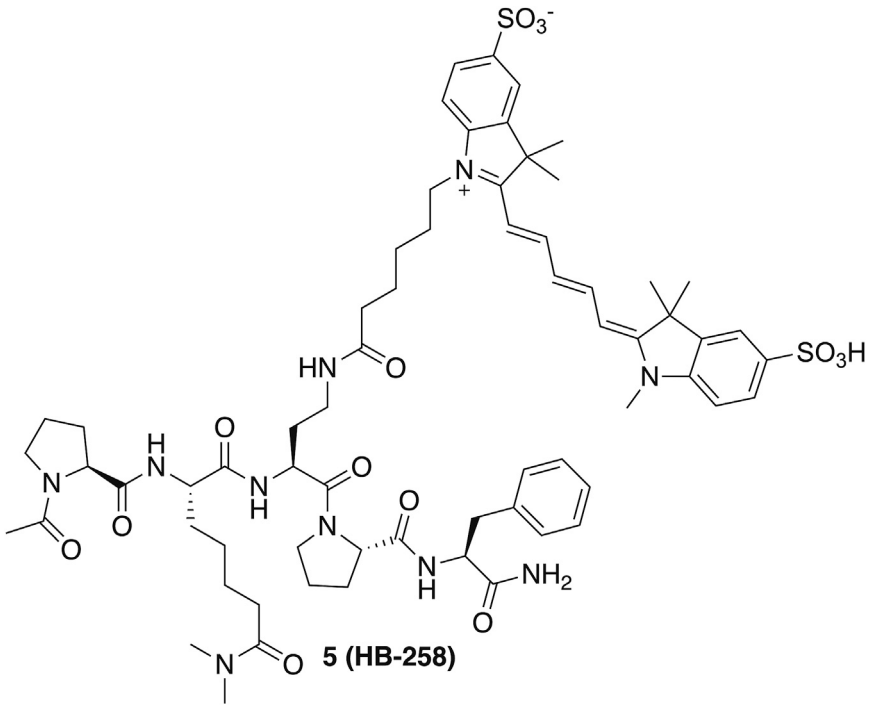

HRMS (ESI) (*m/z*): calculated for $C_{66}H_{88}N_{10}O_{14}S_2$ $[M+2H]^{2+}$: 655.3034 found: 655.3039.

Native-33mer (H-LQLQPFPQPQLPYPQPQLPYPQPQLPYPQPQPF-NH$_2$)

The native-33mer peptide was synthesized according to the general peptide synthesis protocol above with one modification; the coupling steps were performed at 60°C for 15 min (rather than room temperature for 1 h).

HRMS (ESI) (*m/z*): calculated for $C_{190}H_{274}N_{44}O_{46}$ $[M+3H]^{3+}$: 1304.3577 found: 1304.3590.

Deamidated-33mer (H-LQLQPFPQPELPYPQPELPYPQPELPYPQPQPF-NH$_2$)

The deamidated-33mer peptide was synthesized according to the general peptide synthesis protocol above with one modification; the coupling steps were performed at 60°C for 15 min (rather than room temperature for 1 h).

HRMS (ESI) (*m/z*): calculated for $C_{190}H_{274}N_{44}O_{46}$ $[M+3H]^{3+}$: 1305.3471 found: 1305.3443.

SulfoCy5-native-33mer

Native-33mer peptide (H-LQLQPFPQPQLPYPQPQLPYPQPQLPYPQPQPF-Rink resin) bound to Rink resin (150 mg, 20 mmol) was swollen in 10 mL of a 1:1 mixture of DMF and DCM for 15 min (note: all tyrosine residues are protected as their *tert*-butyl ethers and all glutamine residues are protected as their trityl amides before cleavage). Meanwhile, SulfoCy5-carboxylic acid (27.2 mg, 40 mmol, 2 equiv) and HBTU (15.2 mg, 40 mmol, 2 equiv) were taken up in 2 mL of 1:1 DMF:DMSO and allowed to stand, protected from light,

at room temperature for 15 min. The swelling solution was drained from the resin and the activated SulfoCy5 carboxylic acid was added on top. Immediately after, DIPEA (17.4 mL, 100 mmol, 5 equiv) was added to the resin slurry. The resin was allowed to rock, protected from light, at room temperature for 21 h. Subsequently, the coupling solution was filtered off and the resin was allowed to dry over vacuum for 2 h. Peptide cleavage from the resin was carried out as described in the general peptide synthesis protocol above. The product was purified by RP-HPLC (C18 preparative column, 31% B to 51% B over 30 min). The appropriate fractions were combined and lyophilized to yield a blue solid (13.7 mg, 15% yield).

HRMS (ESI) (*m/z*): calculated for $C_{222}H_{310}N_{46}O_{53}S_2$ $[M+3H]^{3+}$: 1512.4231 found: 1512.4227.

SulfoCy5-deadmiated-33mer

Deamidated-33mer peptide (H-LQLQPFPQPELPYPQPELPYPQPELPYPQPQPF-Rink resin) bound to Rink resin (150 mg, 20 mmol) was swollen in 10 mL of a 1:1 mixture of DMF and DCM for 15 min (note: all tyrosine residues are protected as their *tert*-butyl ethers, all glutamine residues are protected as their trityl amides, and all glutamate residues are protected as their *tert*-butyl esters before cleavage). Meanwhile, SulfoCy5-carboxylic acid (27.2 mg, 40 mmol, 2 equiv) and HBTU (15.2 mg, 40 mmol, 2 equiv) were taken up in 2 mL of 1:1 DMF:DMSO and allowed to stand, protected from light, at room temperature for 15 min. The swelling solution was drained from the resin and the activated SulfoCy5 carboxylic acid was added on top. Immediately after, DIPEA (17.4 mL, 100 mmol, 5 equiv) was added to the resin slurry. The resin was allowed to rock, protected from light, at room temperature for 20 h. Subsequently, the coupling solution was filtered off and the resin was allowed to dry over vacuum for 2 h. Peptide cleavage from the resin was carried out as described in the general peptide synthesis protocol above. The product was purified by RP-HPLC (C18 preparative column, 30% B to 50% B over 30 min). The appropriate fractions were combined and lyophilized to yield a blue solid (13.0 mg, 14% yield).

HRMS (ESI) (*m/z*): calculated for $C_{222}H_{307}N_{43}O_{56}S_2$ $[M+3H]^{3+}$: 1513.4071 found: 1513.3274.

Preparation of recombinant human thioredoxin (TRX)

Human TRX was expressed and purified as previously described.[33] Briefly, *E. coli* BL21(DE3) cells harboring a pQE-T7 derivative encoding N-terminally His_6-tagged TRX were induced by adding 200 μM IPTG and grown further for 16 h at 18°C. Cultures were centrifuged at 5000 *g*. Cell pellets were flash-frozen and stored at −80°C overnight. Upon thawing, cells were resuspended in lysis buffer (50 mM NaH_2PO_4, 500 mM NaCl, 10 mM imidazole, pH 7.2). Following sonication, clarified lysates were centrifuged at 20,000 *g* and supernatants were incubated with Ni-NTA resin with 0.5 mL resin per liter culture. Ni-NTA eluates were diluted with MilliQ water, filtered, and purified by anion exchange chromatography with a linear gradient from FPLC Buffer A (20 mM Tris, 1 mM EDTA, 1 mM EGTA, 1 mM DTT, pH 7.2) to FPLC Buffer B (FPLC A + 1 M NaCl) at 4°C. The desired fractions were pooled, concentrated on a 7.5K MWCO Amicon spin concentrator, brought to 20% glycerol, flash frozen, and stored at −80°C.

Preparation of recombinant human transglutaminase 2 (TG2)

Human TG2 was expressed and purified as before.[33] Briefly, *E. coli* BL21(DE3) cells harboring a pET-28a derivative encoding N-terminally His_6-tagged TG2 were induced by adding 200 μM IPTG and grown further for 16 h at 18°C. Cultures were centrifuged at 5000 *g*. Cells were resuspended in lysis buffer (50 mM NaH_2PO_4, 500 mM NaCl, 10 mM imidazole, pH 7.6) and incubated in chicken egg-white lysozyme at a final concentration of 1 mg/mL for 1 h. Following sonication, clarified lysates were centrifuged at 20,000 *g* and supernatants were incubated with Ni-NTA resin with 0.5 mL resin per liter culture. Ni-NTA eluates were diluted with FPLC Buffer A (20 mM Tris, 1 mM EDTA, 1 mM EGTA, 1 mM DTT, pH 7.6), filtered, and purified by anion exchange chromatography with a linear gradient in FPLC Buffer B (FPLC A + 1 M NaCl) at 4°C. The protein eluted at ∼30% FPLC B. The desired fractions were pooled, concentrated on a 30K MWCO Amicon spin concentrator, brought to 20% glycerol, flash frozen, and stored at −80°C.

Purification of truncated TG2 derivatives

Truncations of TG2 with N terminal his-tags were created: TG2-Cβ1 (containing residues 1–586, lacking β2 domain), TG2-Cβ1β2 (containing residues 1–460, lacking β1 and β2 domains).[38] WT and Truncated TG2 were purified as previously discussed.[58] Briefly, TG2 variants were extracted from Rosetta2 cells and purified via a nickel column. Eluant from the nickel column was anion exchanged on a HiTrapQ column using TG2 Anion exchange buffer (20 mM Tris HCl, 1 mM DTT, and 1 mM EDTA, pH 7.2) with a 0–1 M NaCl gradient. Finally, size exclusion chromatography was performed on a Superdex™ 200 pg column using TG2 SEC buffer (20 mM Tris, 150 mM NaCl, pH 8).

Preparation of recombinant human α_2-macroglobulin (α_2M) from mammalian cells

Plasmid for recombinant WT α_2M expression was prepared by synthesizing a sequence based on human α_2M reference sequence NM_000014.4 and cloning it into pcDNA3.1(+) backbone using NheI and XbaI restriction sites. WT α_2M was expressed in Expi293F cells using recommended protocol for the Expi293™ Expression System. Briefly, WT α_2M plasmid was transfected into 2.5×10^6 Expi293F cells in 100 mL Expression Medium by using the ExpiFectamine 293 Transfection Kit and Opti-MEM. After 18–22 h, 600μL of Transfection Enhancer 1 and 6 mL of Transfection Enhancer 2 were added. The cultures were expanded for 5 days to allow for protein expression. 1M HEPES at pH 7.4 was added to the cultured supernatant to a final concentration of 50 mM HEPES. WT α_2M was purified from supernatant in a two-step process. First, a Zinc based ion affinity chromatography was performed on a HiTrap Chelating HP column previously loaded with 10 mL of 100 mM Zinc. The binding buffer for the zinc-based affinity chromatography (50 mM NaCl, 20 mM sodium Acetate, pH 7.4) and eluting buffer (50 mM EDTA, 150 mM NaCl, 100 mM Sodium Acetate, pH7.4). This is followed by SEC purification using a 30mL Sephacryl 400-HR in α_2M running buffer (20 mM HEPES, 350 mM NaCl, pH 7.4).

Preparation of recombinant human receptor associated protein (RAP)

E. coli BL21(DE3) cells were transformed with a pET-21 plasmid encoding C-terminally His6-tagged RAP construct.[43] A single colony was picked and inoculated into 20mL of LB medium supplemented with 100 mg/mL carbenicillin and grown at 37C at 200 rpm overnight. 5 mL of this starter culture was inoculated into 1 L of LB medium supplemented with 100 mg/mL carbenicillin, and the cultures were grown at 37°C at 200 rpm until OD600 reached 0.3 at which point the temperature was decreased to 18°C. The cultures were grown further at this temperature until OD600 reached 0.6 at which point protein expression was induced with 200 mm IPTG. The cultures were incubated for 18 h at 18°C at 200 rpm before the cells harvested by centrifugation (5000 *g* × 20 min, 4°C). The pellets were flash-frozen and stored at −80°C. Cell pellets were thawed and resuspended in 30 mL of lysis/wash buffer (20 mM HEPES, 150 mM NaCl, 25 mM imidazole, 10% glycerol [m/v], pH 8.0) and lysed on ice by sonication. The lysate was clarified by centrifugation (25000 *g* × 75 min, 4°C). The supernatant was decanted onto Ni-NTA resin (3 mL of resin for 4 L of culture) that had been pre-equilibrated to the lysis/wash buffer and allowed to incubate at 4°C for 1 h. The resin was washed three times with 35 mL of lysis/wash buffer each time. Resin-bound protein was eluted twice with 5 mL of Ni elution buffer (20 mM HEPES, 150 mM NaCl, 300 mM imidazole, 10% glycerol [m/v], pH 8.0). The eluate was concentrated using a 10 kDa Amicon concentrator. The protein was further purified by size-exclusion chromatography with SEC buffer (20 mM HEPES, 150 mM NaCl, pH 8.0). Fractions containing the protein of interest were confirmed by SDS-PAGE analysis and were concentrated using a 10 kDa Amicon concentrator, supplemented with glycerol (10% v/v), aliquoted, flash frozen, and stored at −80C. Protein concentration was determined by NanoDrop A280 (extinction coefficient 35,075 M^{-1} cm^{-1}, MW 39163.15 Da).

Kinetic assays

TG2 activity was assayed as previously described.[59] Briefly, a reaction mixture containing 200 mM MOPS (pH 7.2), 5 mM $CaCl_2$, 10 mM α-ketoglutarate, 18 U/mL glutamate dehydrogenase, 0.5 mM NADH, and the indicated concentration of substrate (Ac-PQLPF-NH_2, unless otherwise specified) was prepared. To assess inhibitory potency, the final concentration of substrate was held constant at the indicated concentration and the concentration of inhibitor was varied. Reactions were initiated with the addition of reduced TG2 that had been freshly desalted into PBS. The final concentration of TG2 in the assay was 1 μM and total reaction volumes were 100 μL. Reactions were monitored spectrophotometrically by following the consumption of NADH (340 nm, ε = 6220 cm^{-1} M^{-1}) for 60 min at 25°C. Progress curves were fit to linear equations and the calculated slopes were used to extrapolate steady state reaction rates. All measurements were performed in triplicate.

Cell culture

Mouse embryonic fibroblasts (MEFs) were grown in DMEM and split 1:4–1:6 every 2–3 days. These cells were propagated in 10 cm plates, then seeded into 12- or 24-well glass bottom plates and grown for 3 days prior to treatment. NRK cells were grown in DMEM media and split 1:4 to 1:10 every 2–4 days depending on confluency. 9022 cells were grown in RPMI media supplemented with 10% FBS and 1% PenStrep and split every 1–3 days depending on confluency.

Generation of MEF$^{-/-}$cell line

Primary mouse embryonic fibroblasts (MEFs) were isolated from E14.5 embryos derived from TG2$^{-/-}$ mice.[57] To generate a homogeneous, proliferative cell line, passage 0 MEFs were transformed with lentivirus encoding the simian virus 40 (SV40) large T antigen.

Conjugation α_2M with an NHS-linked fluorophore

A 5 mg/mL solution of purified α_2M was incubated with a 10x molar excess of 555- Alexa fluorophore NHS-ester for 1 h at RT, rocking continuously. The solution was then desalted twice using 7MWKO Zeba spin columns.

Cellular assays – Adherent cells

At the start of each experiment involving NRK or MEF cells, media was replaced with fresh media, and TG2 substrate, α_2M and TRX were added as specified. When using non-peptidic inhibitors (CK805, cystamine, Pitstop), compounds were added to the cell culture 30 min prior to other treatments unless otherwise indicated. After treatment for 1.5 h, cells were washed three times with HBSS and then fixed with 2% paraformaldehyde (PFA) solution in PBS for 10 min at room temperature. The cells were washed 2x with PBS and incubated for 12 min in a 1:1000 DAPI solution, then washed again three times in PBS. If no antibody staining was used, the same protocol was followed starting at the PBST washes. All operations were carried out under low light to minimize photobleaching.

Generation of NRK RFP-LAMP-1 cell line

RFP-LAMP-1 expressing cells were generated as previously described.[60] Briefly, the plasmid carrying RFP-LAMP-1, lentivirus and VSVg DNA was mixed with Bring X-tremeGENE 9 DNA Transfection Reagent (Roche Diagnostics GmbH, #06365779001) and the mixture added to HEK293 T cells to generate an RFP-LAMP-1 lentivirus. NRK cells were treated with the virus and spun at 2200 rpm for 45 min at 37°C. Cells expressing the desired construct were selected using FACS. The clonal populations were grown in DMEM at 5% CO_2 and 37°C until confluent.

Cellular assays – Suspension cells

For experiments involving 9022 cells, 20 mL of cell suspension at ~10^7 cells/mL were pelleted at 400 *g* for 5 min. The cells were re-suspended in 5mL fresh RPMI media and 200μL of the suspension was added to each well in a poly-L-lysine coated 24-well glass bottom plate. The cells were allowed to settle and adhere for 20 min at 37°C. HB230 or Cy5-33mer, α_2M, and 100 nM TG2 were then added, as specified, and incubated for 2.5 h. Cells were washed gently with RT PBS and stained with SVL-3 mouse anti-human antibody at a 1:50 dilution and/or a custom anti-TG2 rabbit anti-mouse (cross-reactive with human TG2) polyclonal antibody at a 1:100 dilution, for 20 min on ice. After washing with PBS, the cells were stained with a secondary antibody (488-Alexa Fluor conjugated rabbit anti-mouse secondary antibody and/or 555-Alexa Fluor conjugated goat anti-rabbit secondary antibody) for 20 min on ice. Cells were washed again, fixed, and stained with DAPI, as described for adherent cells.

Isolation and differentiation of BMDC and BMM

The tibia and femur were removed from female C57BL6 or TG2KO mice, and the bone marrow cells were flushed out using a 1 mL syringe with a 26G needle filled with PBS. Red blood cells were removed, and BM cells were resuspended in 6 mL complete media (RPMI supplemented with 10% FBS and 1% PenStrep) and plated in a Petri dish at a density of 8 × 10^6 cells in complete medium with 20 ng/mL GM-CSF per plate for BMM differentiation. To generate BMM, added 3 mL of complete medium plus 20 ng/mL MCSF on day 2 and day 4, then harvested adherent cells using 5 mM EDTA on day 5. To generate BMDC, bone marrow cells were resuspended in 10 mL complete media with 10 ng/mL GM-CSF at a density of 2 × 10^6 cells per 10-cm Petri dish. Added 10 mL of 10 ng/mL GM-CSF-containing complete media on day 3 and 6, then harvested suspension cells on day 8.

Confocal immunofluorescent microscopy

Cells were imaged on an LSM780 confocal fluorescence microscope using up to 4 channels. The microscope was equipped with a 63x oil immersion lens. HB230 and Cy5-33mer was detected on the red channel (647 nm), whereas α_2M was observed on the green channel as was the secondary antibody for TG2 (555 nm). HLA-DQ2 was visualized using an SPV-L3 mouse antibody (Novus Biologicals) and a secondary rabbit anti-mouse secondary antibody conjugated to an Alexa Fluor (488 nm). The nuclear stain DAPI was visualized on the blue channel (405 nm).

QUANTIFICATION AND STATISTICAL ANALYSIS

Calculation of kinetic parameters

Progress curves were fitted to linear equations and the calculated slopes were used to extrapolate steady state reaction rates by fitting to the Michaelis-Menten equation in GraphPad Prism 9. All measurements were performed in triplicate.

Colocalization analysis

Colocalization analysis was performed using Coloc2 and Colocalizecolocalization tools in Fiji (ImageJ).

HB230-containing vesicles quantification in NRK cells

Using the particle analysis tool in Fiji (ImageJ) the number of particles in the HB230 (647 nm) channel were quantified. Circularity cut-off was set at 0.3 and minimum size of particles was 0.1 μM. The number of vesicles was normalized to the number of cells as measured by DAPI staining and plotted in GraphPad Prism 9.

Quantification of antigen presentation by 9022 cells

2–4 frames of 3–6 experimental replicates were analyzed for each condition. Cells were counted if they had a well-defined nucleus and clearly defined expression of HLA-DQ2. Cells with overlay of HLA-DQ2 antibody and Cy5-33mer in at least one section of the cell surface counted as presenting Cy5-33mer on MHC-II.

Statistical analysis

For all datasets, data from different samples was compared using Student's *t* test pairwise comparison when comparing two conditions, or one-way ANOVA when comparing multiple conditions. Statistical significance: *$p < 0.05$, **$p < 0.01$, ***$p < 0.001$, ****$p < 0.0001$. Comparisons generated in GraphPad Prism 9. Points were plotted as mean ± SD No additional methods were used to determine whether data met the assumptions of the statistical approach beyond the built-in methods in the GraphPad Prism 9 analysis tools.

Statistical details of experiments can be found in the figure legends.